LBL-1531

STUDY OF A BEAM-PLASMA INSTABILITY BY SPECTROSCOPIC METHODS

Roger A. Hess

(Ph. D. Thesis)

December 1972

Prepared for the U. S. Atomic Energy Commission under Contract W-7405-ENG-48

LBL-1531

DISCLAIMER

STUDY OF A BEAM-PLASMA INSTABILITY BY SPECTROSCOPIC METHODS

Contents

STUDY OF A BEAM-PLASMA INSTABILITY BY SPECTROSCOPIC METHODS

Roger A. Hess

Lawrence Berkeley Laboratory
University of California
Berkeley, California 94720

December 1972

ABSTRACT

Spectroscopic methods are used to study a beam-plasma system and in particular the electric fields produced by the beam-plasma instability. A 4 keV, 40 mA electron beam of diameter 1 mm is directed into a chamber containing He at 0.3 Torr pressure. An external magnetic field of up to 7600 G is present. The electron beam can be chopped for time-resolved measurements on the initial growth of the beam-plasma instability; the rise time of the beam is 10 nsec and the fall time is 100 nsec.

The plasma is initially produced by the direct collisional ionization of the neutral helium by the beam electrons. An unstable interaction then forms between the beam and plasma which results in large electric fields. These electric fields heat the plasma electrons to the point where they produce further ionization. The plasma has a maximum density of $n_e \approx 5 \times 10^{13}$ cm^{-3}, an electron temperature $T_e \approx 5$ eV, and an ion temperature $T_i < 0.15$ eV. The basic parameters of the plasma are shown to be reasonably self-consistent, taking into account mechanisms for the generation and loss of charged particles.

The combined high-frequency Stark and Zeeman effects are used to make time and spatially resolved measurements on the

electric fields due to the beam-plasma interaction. A brief review is given of the theory of the Stark-Zeeman effect and its use as a tool for plasma diagnostics is discussed. Electric fields induce transitions which appear as "satellites" of normally forbidden spectral lines. The frequency, polarization, and amplitude of the electric fields can be deduced from examination of these satellites.

Time resolved measurements show that the electric field of the instability grows from noise level to near saturation within a time $\approx$ 25 nsec after the beam is turned on. The electric field is nearly entirely confined to the volume traversed by the electron beam, and has its maximum amplitude on the edge of the beam. The electric field is also strongly localized in the axial direction along the beam with a peak at a distance of 2-4 cm from where the beam enters the chamber. After saturation of the instability, the field has a maximum aplitude of about 2000 V/cm. The frequency of the electric field is measured to be near to 74 GHz and could be either the electron plasma frequency or the upper hybrid frequency within errors on knowledge of the density. The frequency spectrum of the electric field is found to be quite narrow; its relative bandwidth is $\lesssim$ 14%. Two different polarizations of the electric field are observed: In one case the electric field is polarized randomly in direction and in another case is polarized perpendicular to the magnetic field and random in azimuthal angle. The two different polarizations are observed for nearly the same beam and plasma parameters. These observa-

vations on the electric field are found to be generally consistent with the results of theoretical studies on the beam-plasma system.

I. INTRODUCTION

The interaction between a charged-particle beam and a plasma, and the instabilities due to this interaction, have been one of the most extensively studied areas within plasma physics. In spite of the many investigations of the beam-plasma instability, both theoretical and experimental, there is still a need for further research due to the variety of the possible interactions and the many parameters which are necessary to describe the beam-plasma system in a realistic case.

Beam-plasma interactions have received so much attention for several reasons: First, the beam-plasma interaction is the simplest velocity-space instability which occurs in plasma physics, and for that reason it provides a useful tool for studying the linear and nonlinear properties of these instabilities. Second, beam-plasma interactions are easy to produce and study in the laboratory. Third, beam-plasma interactions are important in several of the applied areas of plasma physics, such as the amplification and generation of microwaves, new methods for the acceleration of charged particles (the electron-ring accelerator), the injection of charged particles into magnetic traps, and the heating of plasmas.

The theory of beam-plasma interactions has several levels of sophistication. The most simple theory is obtained for an infinite, cold, collisionless plasma; an infinite, monoenergetic, weak beam (beam particle density much less than plasma particle density); and no external electric or magnetic fields. Even

then the theory is only amenable to analytic solution in the linear regime. The theory can be simplified by assuming an infinite magnetic field along the beam so as to limit the motion of the beam and plasma particles to one dimension.

Unfortunately, few of the above conditions are realized in a laboratory plasma, although some of them may be closely approximated. It is valid to ignore the effects of finite size of the beam or plasma if the wavelengths of interest are much smaller than the dimensions of the system. Electron beams with a small velocity spread can be produced, and a plasma can be treated as cold if the beam velocity is very much larger than the thermal velocities of the plasma electrons. Laboratory plasmas are often immersed in magnetic fields and these fields can seldom be considered as infinite. Also, collisions must be considered, both collisions between charged particles and neutrals, and Coulomb collisions.

In the experiment described in this paper, the beam consists of a 4 kV electron beam with a diameter of 1 mm and a current density of approximately 5 A/cm^2. The electron beam can be pulsed in order to investigate the initial growth of the beam-plasma instability. The plasma is produced by the beam itself, originally by direct collisional ionization of the background gas (helium at a pressure of 0.3 Torr) by the beam electrons; subsequently by ionizing collisions of plasma electrons heated by the electric fields of the beam-plasma interaction. The interaction occurs in an external magnetic field of up to 7600 gauss.

Thus, the analysis of this beam plasma suffers from some of the difficulties mentioned above. Furthermore, a thorough understanding of the processes occurring in the plasma must include other plasma properties such as ionization, recombination, diffusion, conduction, and radiation. With all of these effects to take into account a detailed comparison between theory and experiment is quite difficult. In addition, the experimental investigation of the beam-plasma system is hampered, as are most investigations in plasma physics, by a lack of good diagnostic techniques.

The present work has two main objectives. One is to produce a detailed description of the beam-plasma system referred to above. This description includes not only information about the interaction itself, but also the plasma which is produced by the instability. The other objective is to study the interaction, in particular the high-frequency electric fields which are produced by the instability, by the use of a recently developed spectroscopic technique, the high-frequency Stark-Zeeman effect, which enables the frequency, amplitude, and polarization of electric fields in a plasma to be measured.

In Chapter II of this paper a review is made of some of the theoretical and experimental results concerning the beam-plasma interaction. Due to the extensive literature on the subject, the review is in no way complete, but is limited to those papers which were considered most relevant to the actual system studied. Chapter III is devoted to the theory of the high-frequency Stark-Zeeman effect and its use as a plasma diagnostic. Chapter IV

consists of a description of the apparatus, the experimental procedure, and the data analysis technique. Chapter V gives the results of the experimental study and a description of the beam-plasma system. The summary and conclusions are given in Chapter VI.

II. BEAM-PLASMA PHYSICS

This chapter is a brief review of some aspects of theoretical and experimental work on the beam-plasma interaction. Aside from a brief historical background, it is restricted to those areas which were considered most pertinent to the experiment which is described in the following chapters, and, in particular, only high-frequency interactions are covered. There have been several reviews in the literature, among them Fainberg[1] and Briggs,[2,3] which cover a wider range of topics in more detail, and include a more extensive bibliography. In Sections B and C of this chapter the references listed are not always the original ones for the given results, but are, in general, more modern and complete sources.

A. Historical Background

Perhaps the first observation of the effects of the beam-plasma instability was made by Langmuir[4] in 1925 during his investigation of the low-pressure plasma diode. In this device a plasma is formed by ionization of a background gas by a beam of electrons of low energy (20 to 100 volts); Langmuir noticed that the electron beam was scattered in distances short compared to the collision mean-free-path.

Langmuir suggested that this anomalously high scattering, now known to be caused by electric fields amplified from noise by the beam-plasma instability, might be due to oscillations of some type. Tonks and Langmuir[5] elaborated on this idea by introducing the theory that the charged particles in a plasma would

tend to oscillate at a characteristic frequency, now known as the plasma frequency. However, they did not extend their ideas to find what effect a stream of electrons would have upon the plasma oscillations.

In 1939 Merrill and Webb[6] studied the scattering of electrons in a plasma and observed oscillations whose frequency agreed with the formula derived by Tonks and Langmuir. The periodic oscillations were found only in regions traversed by fast electrons and the results were interpreted as showing that the anomalous electron scattering was due to plasma oscillations which received their energy from the beam electrons.

The first theoretical treatment of the beam-plasma instability was given by Pierce.[7,8] He found that an electron beam with a neutralizing background of stationary or nearly stationary ions could support growing waves at frequencies near the ion plasma frequency. Similar results were found by other investigators[9-11] in connection with research on tubes designed for the generation and amplification of microwaves, although in these cases the growing waves occurred near the electron plasma frequency since the interaction took place between beam and plasma electrons.

Bohm and Gross[12] also made a theoretical study of the beam-plasma system. They found that collisions would tend to damp the waves and hence act as a stabilizing influence, an effect that was also discussed by Pierce.[7]

Looney and Brown[13] failed in one of the first deliberate

attempts to excite plasma oscillations by means of the beam-plasma interaction. Their failure has been explained[1] as being due to the low level of the initial perturbations and the small amount of amplification permitted by the experimental conditions.

The first clear demonstration of spatial growth of waves under conditions where the linear theory was valid was made by Boyd et al.[14] They used a thin weak beam that was modulated by means of a microwave signal. When the modulation of the beam was measured after traversing a separately maintained plasma, amplification was observed, and was found to be greatest when the frequency of modulation equalled the plasma frequency of the plasma.

The first quantitative observations of the beam-plasma instability with a beam that was not premodulated were made by Kharchenko et al.[15]

B. Linear Theory

The linear theory of the beam-plasma interaction provides information about the initial response of the system to a small perturbation from equilibrium, but it provides no information about the final state of the system if a perturbation does grow. Due to its greater simplicity, the linear theory has been more highly developed than nonlinear theory.

In the linear analysis of the beam-plasma interaction, the response of the system is sought to a perturbation in which the perturbed quantities vary as $e^{i(\vec{k}\cdot\vec{r}-\omega t)}$. The result is a dispersion relation, that is, a relation between ω, the frequency, and k, the wavenumber of the wave.

There are two ways of considering the dispersion relation to determine if the wave is stable or unstable. The first is to consider k as real and ω as complex; in this case the temporal evolution of the perturbation is determined by the imaginary part of ω. Alternatively, ω may be considered as real, and k as complex; then the spatial growth or decay of the wave is determined. While plasma theorists usually consider ω as the complex variable, microwave theorists and experimentalists studying the beam-plasma interaction are generally more interested in knowing the imaginary part of k, as it is the spatial growth rate of an instability which is most easily measured in most cases.

The two ways of considering the dispersion relation are related to the distinction between absolute and convective instabilities: When a system is perturbed by a pulse that is originally of finite spatial size, the pulse may grow at every point of space (absolute instability) or it may propagate along the system so that at each point the disturbance will first grow and then decay as the pulse passes the point (convective instability). Briggs[3] has developed criteria for determining from the dispersion relation whether an instability is convective or absolute.

The dispersion relation for an infinite, homogeneous, one-dimensional, cold, collisionless beam-plasma system is given by[3]

$$1 - \frac{\omega_p^2}{\omega^2} - \frac{\omega_b^2}{(\omega - ku)^2} = 0. \qquad (1)$$

Here, ω_p and ω_b are the plasma frequency of the plasma and beam,

respectively, and u is the velocity of the beam. It is found from this equation that the plasma is unstable (that is, there are solutions for complex ω corresponding to growth for k real) for

$$|k| < \frac{\omega_p}{u}(1 + \eta^{1/3})^{3/2},$$

where

$$\eta \equiv \frac{\omega_b^2}{\omega_p^2} = \frac{n_b}{n_p}.$$

Here, n_b and n_p are the number density of electrons in the beam and plasma. Equation (1) has been found by Briggs[2] to be neither a purely convective nor purely absolute instability but represents a border-line case.

In what follows in this section, the weak beam assumption is made, that is, $\eta \ll 1$. In fact, the stronger condition $\eta^{1/3} \ll 1$ is also assumed since it is $\eta^{1/3}$ that often appears as an expansion parameter.

Although Eq. (1) predicts instability for a wide range of k, in practice the fastest growing wave will be the one that is observed. When Eq. (1) is solved subject to the condition that Im(ω) is a maximum, the result is[16]

$$\begin{aligned} &\mathrm{Re}(\omega) = \omega_p(1 - 2^{-4/3}\eta^{1/3}) \\ &k_0 \equiv \omega_p/u \\ &\gamma_0 \equiv \mathrm{Im}(\omega) = 3^{1/2}2^{-4/3}\eta^{1/3}\omega_p \\ &V_g = \frac{\partial\omega}{\partial k} = \frac{2}{3}u. \end{aligned} \tag{2}$$

The expressions are correct to first order in $\eta^{1/3}$. We can see from these results that the oscillation frequency is very close to the plasma frequency, the growth rate is much less than the plasma frequency, and the phase velocity of the wave is very close to the beam velocity.

When Eq. (1) is solved for complex k as a function of real ω, it is found that $k_i \to \infty$ as $\omega \to \omega_p$. Thus, in a real situation, the spatial growth rate must be limited by other effects.

When collisions of the plasma particles and beam temperature are taken into account, the dispersion relation becomes[2]

$$1 - \frac{\omega_p^2}{\omega(\omega + i\nu_c)} - \omega_b^2 \int_{-\infty}^{+\infty} \frac{f_0(v)dv}{(\omega - kv)^2} = 0. \qquad (3)$$

Here ν_c is the collision frequency of the plasma electrons, and $f_0(v)$ is the distribution function of the beam electrons. This can be simplified to an algebraic equation by assuming a Lorentzian distribution function

$$f_0(v) = \frac{\Delta u/\pi}{(\Delta u)^2 + (v - u)^2}, \qquad (4)$$

where Δu is the half-width of the distribution function. Then Eq. (3) becomes

$$1 - \frac{\omega_p^2}{\omega(\omega + i\nu_c)} + \frac{\omega_b^2}{\left[k\Delta u - i(\omega - ku)\right]^2} = 0. \qquad (5)$$

If the collisions alone are considered (that is, $\Delta u = 0$),

the temporal growth is reduced in the limiting case[17] $\nu_c \gg \gamma$ to

$$\gamma = \gamma_0 \frac{2^{1/2}}{3^{3/4}} \left(\frac{\gamma_0}{\nu_c}\right)^{1/2}, \tag{6}$$

where γ_0 is the collisionless growth rate defined in Eq. (2).

When both collisions and the beam temperature are included in the dispersion relation, the maximum spatial growth rate is[18]

$$k_i = \frac{1}{1 + \left(\frac{\Delta u}{u}\right)^2} \left[\frac{3^{3/4}}{2^{3/2}} \left(\frac{\eta\omega_p}{\nu_c}\right)^{1/2} - \frac{\Delta u}{u}\right] \frac{\omega_p}{u}, \tag{7}$$

where it has been assumed that $\nu_c \ll \omega_p$ as well as $\eta \ll 1$. Thus, k_i changes sign, and the instability is quenched when

$$\frac{\nu_c}{\omega_p}\left(\frac{\Delta u}{u}\right)^2 > 0.65\eta. \tag{8}$$

Thus, although collisions alone do not suppress the beam-plasma instability, it may be suppressed if the beam has a finite temperature. Collisions can actually increase the growth rate for some frequencies as strong collisional damping results in an instability due to the growth of a negative energy wave.[19]

When the effects of finite beam size are included, but collisions and thermal effects are ignored, the dispersion relation becomes[20]

$$1 - \frac{\omega_p^2}{\omega^2} - \frac{\omega_b^2}{(\omega - ku)^2} G_m(kR) = 0. \tag{9}$$

R is the radius of the beam, assumed to be much less than the radius of the plasma, and the perturbation is assumed to vary as exp $i(\omega t - m\theta - kz)$, where z is the coordinate parallel to the beam axis, θ is the azimuthal angle about the beam axis, and m is an integer. $G_m(kR)$, known as the plasma frequency rduction factor, is a complicated function of its argument involving Bessel functions of order m, but $G_m(\infty) = 1/2$ for all m and its values range from 0 to 1/2 for all m and R. Thus, the dispersion relation Eq. (9) is identical to Eq. (1) except that the beam density is effectively reduced by the factor G_m. Although the dispersion relations Eq. (1) and Eq. (9) look similar, the interaction in the two cases is qualitatively different. For the unbounded system, the beam waves are body waves, while for the finite beam they are surface waves associated with the beam edge.[20]

When the effect of a finite external magnetic field is included, the dispersion relation becomes even more complicated, as then the waves on the beam can interact with the cyclotron waves of the plasma. The dispersion relation has been calculated[21] and in the weak-beam limit it has solutions only in the vicinity of frequencies satisfying simultaneously the cold plasma dispersion relation,

$$\left(\frac{k_{\parallel}c}{\omega}\right)^2\left(1 - \frac{\omega_p^2}{\omega^2}\right) + \left(\frac{k_{\perp}c}{\omega}\right)^2\left(1 - \frac{\omega_p^2/\omega^2}{1 - \omega_c^2/\omega^2}\right) = 0, \qquad (10)$$

and the synchronism condition

$$\omega - m\omega_c - k_{\parallel}u = 0. \qquad (11)$$

Here ω_c is the electron cyclotron frequency and m is again an integer. The perturbed quantities are assumed to vary as $\exp i(k_{\parallel}z + k_{\perp}x - \omega t)$, where x is a coordinate perpendicular to the beam axis. Clearly, Eq. (11) shows that the interaction is due to a resonance between the Doppler shifted wave and a cyclotron harmonic.

Unstable solutions for ω are found for m = 0 and m = -1, and for the conditions of the present experiment, the m = 0 mode grows faster. Its temporal growth rate is[21]

$$\gamma = \omega \frac{\sqrt{3}}{2} B^{1/3}$$

$$B \equiv \frac{1}{2}\frac{\omega_b^2}{\omega_p^2}\frac{(\omega^2 - \omega_c^2)^2}{(\omega^2 - \omega_c^2)^2 + (k_{\perp}u)^2\omega^2} \tag{12}$$

and the excited frequency is given by the solution of the equation

$$\omega^2 - \omega_p^2 = \frac{\omega_c^2}{1 + (\omega^2 - \omega_c^2)/(k_{\perp}u)^2} . \tag{13}$$

For $\omega_c = 0$ and $k_{\perp} = 0$, we recover the results of Eqs. (2). Solutions of Eq. (13) for various values of the parameter $k_{\perp}u/\omega_c$, including the effects of beam and plasma temperatures are given by Seidl.[22] For the conditions of the present experiment, the results of Seidl show that the beam and plasma temperatures do not become important until $(u_t/u)^2 > 10^{-2}$, where u_t is the mean spread in velocity of the beam or plasma.

C. Nonlinear Theory

Linear theory predicts that the beam-plasma instability will grow exponentially in time or space, but it does not predict when or how that growth stops, or the state of the system at saturation. While nonlinear theories have been formulated to attempt to answer these questions, the results are not as quantitative as those of the linear theory, and complications that arise due to finite geometry, magnetic fields, and collisions have not as of yet been included in the theories.

All of the nonlinear theories find qualitatively the same results: The basic nonlinear effect is the distortion of the beam distribution function. If the beam is originally monoenergetic, the effect of the instability will be to smear out the distribution function (lowering the average beam velocity), and, as was shown for the linear case, Eq. (7), this smearing leads to a reduction in the growth rate.

The physical picture that has been developed[16,23-26] for the initial saturation of the instability is known as the single-wave model, as its essential point is that the beam electrons interact with a nearly sinusoidal wave of a single frequency.

The linear dispersion relation, Eq. (1), which describes the initial interaction predicts that the growing band of wavenumbers, and hence frequencies, will be quite narrow. The half-width of the peak growth rate is[24]

$$\Delta k = \left(\gamma_0 \left| \frac{\partial^2 \gamma}{\partial k^2} \right| \right)^{-1} = \frac{3}{2^{5/6}} \eta^{1/3} k_0. \tag{14}$$

That is, at $k = k_0 \pm \Delta k$, the growth rate is $\frac{1}{2} \gamma_0$, where γ_0 and k_0 are defined in Eq. (2). Since $\eta^{1/3} \ll 1$ is assumed, the relative band width is small and as the instability grows the spectrum will become even more peaked.

The velocity of the beam with respect to the wave is small:

$$\Delta v = u - \frac{\omega}{k} = 2^{-4/3} \eta^{1/3} u. \tag{15}$$

Therefore the beam electrons see a single coherent wave at the frequency and wavenumber of maximum growth, and as the wave grows it eventually reaches an amplitude at which it can trap the beam electrons. At that point the linear theory breaks down and the instability begins to saturate. When the electrons become trapped they begin to rotate in phase space with the frequency $\omega_p \eta^{1/3}$ and the electric field amplitude oscillates with the same frequency. The oscillations become damped as the beam distribution function becomes even more smeared out, and the energy in the electric field approaches a constant value[23]

$$\frac{E^2}{8\pi} \approx 2^{-4/3} \eta^{1/3} (n_b m u^2/2). \tag{16}$$

Thus, the wave processes that occur are: fast initial growth at the linear rate, saturation, and damped oscillation. These results have been confirmed by other authors[16,24-26] by means of

computer simulation.

The further evolution of the beam-plasma instability has been investigated[25,27] using quasilinear theory. The beam distribution is further distorted until it becomes close to a plateau in velocity space in times of the order

$$t \sim (\omega_p \eta)^{-1} \tag{17}$$

and close to Maxwellian in times

$$t \sim \omega_p^{-1} \eta^{-4/3}. \tag{18}$$

Both (16) and (17) should be taken as very rough estimates.

A recent computer simulation experiment[28] has explored the long-time evolution of the beam plasma instability. It was found that for low density beams ($\eta \ll 0.038$), after the initially most unstable wave grows and saturates, the electric field energy continues to grow slowly, approximately linearly with time, up to a time $t \approx 500\ \omega_p^{-1}$ (this was as far as the numerical calculations were carried).

D. Experimental Studies of Beam-Plasma Instabilities

Some of the first experiments on a beam-plasma system in a magnetic field were done by Kharchenko et al.[29-31] who found that instabilities excited oscillations in the beam and plasma whose frequency was close to $\omega_H \equiv (\omega_p^2 + \omega_c^2)^{1/2}$, the upper hybrid frequency.

Berezin et al.[32,33] made measurements on the velocity distribution function of a beam and, as expected, it was flattened

after the beam had passed through a region containing a plasma with which it interacted. They also used microwave methods to measure the electric field strengths generated by the instability and found fields of 1 to 2 kV/cm for longitudinal waves and 70 to 100 V/cm for transverse waves.

Böhmer et al.[17,18] also made measurements of the beam distribution function. They found that the flattening was a maximum for a particular plasma density and was less for both higher and lower plasma densities, and they interpreted this as evidence for damping of the wave due to Coulomb collisions. They also found that heating of the plasma by the instability increased the density at which the beam was flattened most, which they cited as further evidence for collisional damping since the Coulomb collision frequency is a sensitive function of electron temperature. In addition they made a study of the effect of collisions when the beam had an initial velocity spread. They confirmed the theoretical prediction of Singhaus[34] that the instability could be quenched by collisions if the energy spread in the beam was sufficiently large.

Generally good agreement was found in two experiments to test linear dispersion relations. Self[35] found that the growth of the instability was somewhat slower and spread over a wider frequency band than the theory predicted, but this was attributed to the radial inhomogeneity of the plasma. Apel[36] found reasonable agreement between the measured frequency, wavelength, and axial growth rate of the instability with those predicted by a disper-

sion equation taking into account the geometry, the magnetic field, and collisions, but neglecting temperature.

Seidl and Sunka,[21] in a measurement on a beam-plasma instability in a magnetic field, found oscillations which approximately followed the upper hybrid frequency, but frequencies in the vicinity of the electron cyclotron harmonics were strongly preferred. They also noticed that during the initial buildup of the plasma after the beam was turned on, the plasma density grew in discrete steps such that the upper hybrid frequency was an integral multiple of the electron cyclotron frequency.

Gentle and Roberson[37] and Mizuno and Tanaka[38] have verified some aspects of the single-wave model of the nonlinear development of the beam-plasma instability. They found that the relative bandwidth of the frequency of the unstable wave was less than 2% and was coherent for 20 to 30 wave periods, long enough for the beam electrons to be trapped. They also confirmed the value of the peak wave energy, Eq. (16), and the scaling of the energy with the beam current.

III. THE HIGH-FREQUENCY STARK-ZEEMAN EFFECT

In the previous chapter it was found that the beam-plasma instability can produce high-frequency oscillations. The oscillating quantities include not only the density of the charged particles in the plasma but also the current density and electric field. The present chapter is concerned with the effect of these electric fields upon the light radiated from the plasma, and since external magnetic fields are so often present in both natural and laboratory plasmas, the combined effect of these two fields is also considered. As will be seen from the following, the light that is radiated allows the determination of several parameters of the electric field including its frequency, amplitude, and direction, and for this reason it becomes a useful diagnostic tool for studying plasmas in general and the beam-plasma interaction in particular. The following section will only outline the underlying theory as previous papers[39-44] have covered it in detail.

A. Perturbation Theory

To find the effect of a high-frequency electric field upon the radiation emitted from the plasma, the effect on the atomic systems which are present in the plasma must be known. Several authors have used quantum mechanical time-dependent perturbation theory to solve the problem. This involved treating the high-frequency electric field and the static magnetic field as small quantities compared to the internal fields which determine the unperturbed energy levels of the atom. Schrödinger's equation becomes

$$i\hbar \frac{\partial \psi}{\partial t} = H_0 + H_1 + H_2(t)\ \psi, \tag{19}$$

where H_0 is the Hamiltonion of the unperturbed atom, H_1 is the interaction energy between the atom and the magnetic field (time independent), and $H_2(t)$ is the interaction energy of the high-frequency external electric field. Assuming the electric field has a harmonic time dependence at a single frequency ω_0, second-order time-dependent perturbation theory has been used to find the spectrum due to the spontaneous emission of an optical photon simultaneous with the induced absorption or emission of a photon from the electric field. The process can be described as follows (see Fig. 1): An atom in state i makes a transition to another state k for which $i \rightarrow k$ is forbidden for electric dipole transitions, but for which $i \rightarrow j$ and $j \rightarrow k$ do have non-zero dipole matrix elements. The electron in state i absorbs or emits a photon from the external electric field in making the transition to the intermediate state j (energy does not have to be conserved in this transition since j is a virtual state), and then decays to the state k with the emission of an optical photon of energy $E_i - E_k \pm \hbar\omega_0$, where E_i and E_k are the energies of states i and k.

The spectrum that is observed is shown in Fig. 2. The line at $\omega_{jk} \equiv (E_j - E_k)/\hbar$ is due to the allowed transition $j \rightarrow k$. ω_{ik} is where the transition $i \rightarrow k$ would appear if it were an allowed transition. The lines at $\omega_{ik} \pm \omega_0$, called "satellites" of the forbidden line, are due to the two quantum transitions, and are weak compared to the line $j \rightarrow i$, as they must if the perturbation

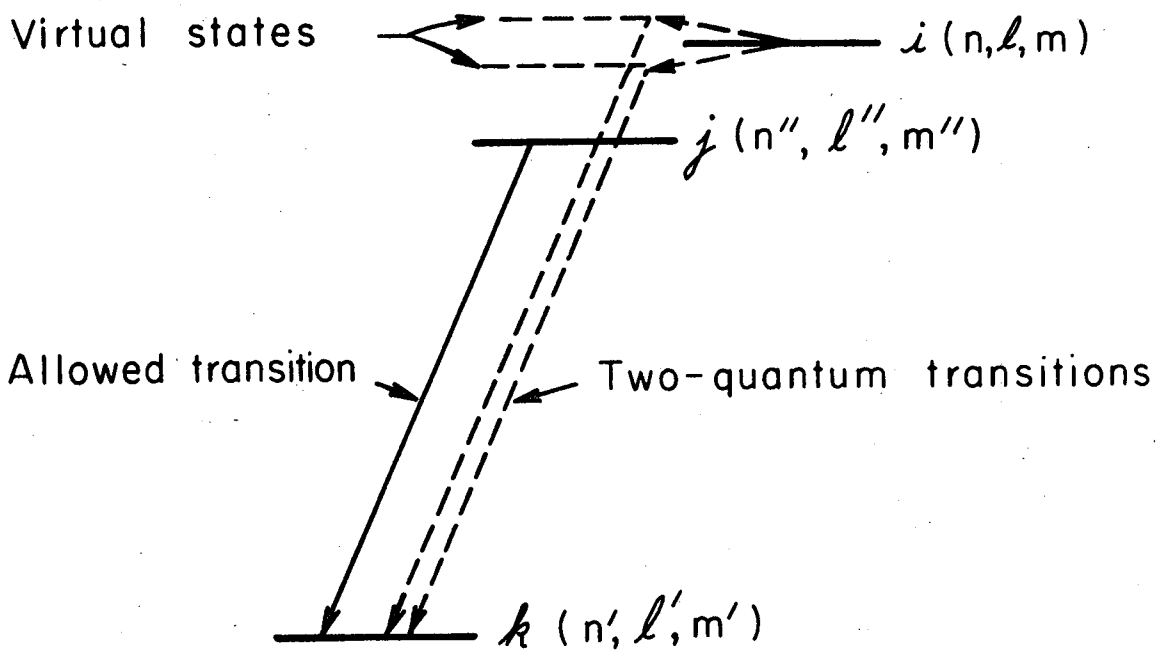

XBL685-2778

Fig. 1. Energy level diagram showing an allowed transition and two-quantum transitions via virtual states.

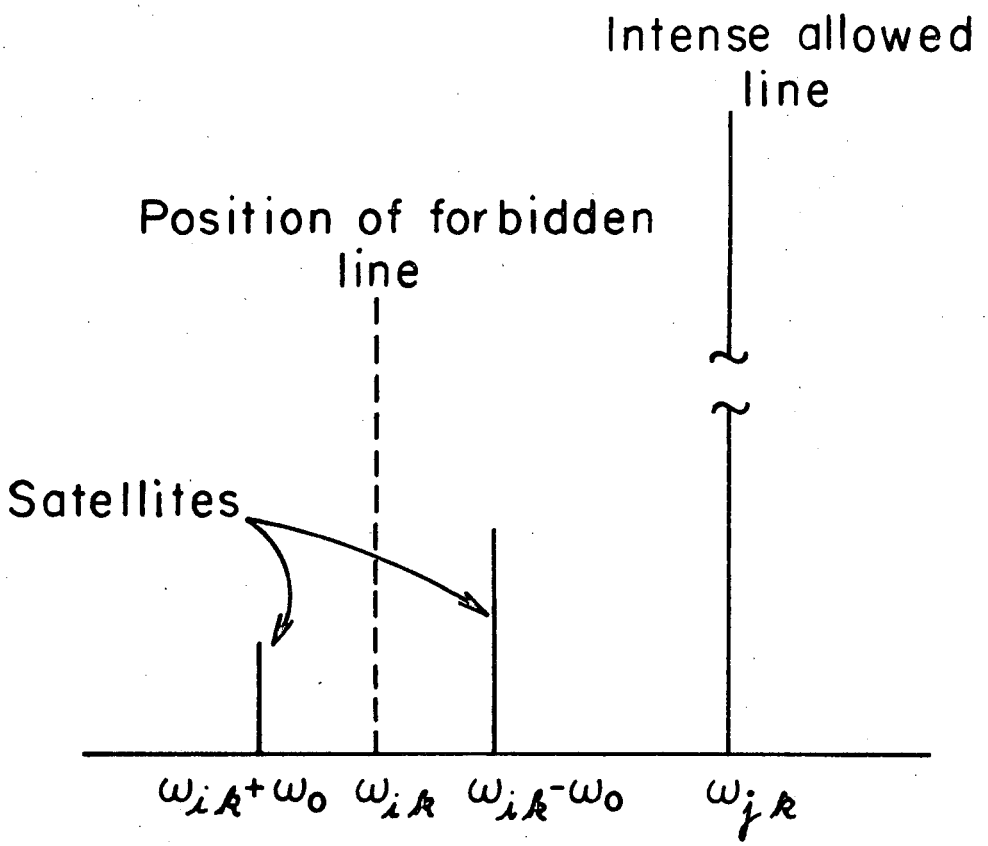

XBL685-2777

Fig. 2. Spectrum due to the transitions shown in Fig. 1.

treatment is to be valid. The ratio of the intensity of these satellites to the intensity of the allowed line for no magnetic field and an electric field that is random in direction is[39]

$$S = \frac{\hbar^2}{6m^2e^2} R_{ij} \frac{E_{rms}^2}{(\omega_{ij} \pm \omega_0)^2} . \qquad (20)$$

It has been assumed that there is only one intermediate state j that is close to the initial state i (otherwise there would be a sum over the intermediate states), E_{rms} is the rms average of the external electric field, and R_{ij} is a dimensionless constant proportional to the oscillator strength of the transition $i \rightarrow j$. The ratio with the upper (lower) sign corresponds to the satellite which is farther (nearer) to the allowed line.

Application of the perturbation theory including other polarizations of the electric field and a static magnetic field has been carried out and the results are given in Ref. 44. When a magnetic field is present each satellite breaks up into a series of lines separated by integral multiples of the Larmor frequency; these Zeeman patterns are strongly dependent on the polarization of the electric field with respect to the magnetic field. Figure 3 (from Ref. 44) shows the relative intensities of the Zeeman components of the satellites for five different electric field polarizations. The direction of observation is perpendicular to $\vec{B}$, and the π and σ components represent light polarized parallel and perpendicular to $\vec{B}$, respectively. The patterns shown were calculated for a magnetic field of 7000 G and an rms electric field of 1000 V/cm. The allowed line (at $\Delta\lambda = 0$ in the figure) is the

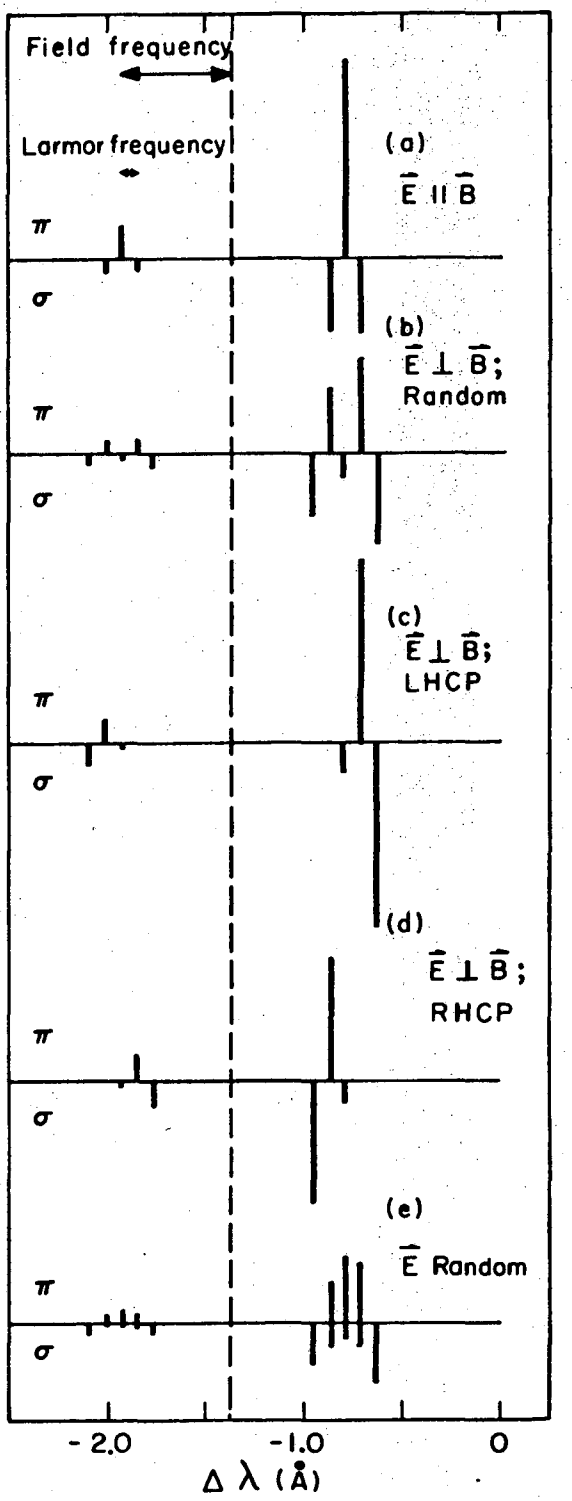

XBL707-3439A

Fig. 3. Theoretical spectra due to two-quantum transitions in magnetic field for five different polarizations of the external magnetic field.

4922 Å ($4^1D - 2^1P$) line of He I. The forbidden line, whose position is indicated by the dotted line in Fig. 3, is the $4^1F - 2^1P$ transition and is -1.35 Å from the allowed line. The integrals over the radial eigenfunctions that were needed to determine R_{ij} were calculated using hydrogenic wavefunctions for the excited electron. Patterns similar to these have been calculated for the dc Stark-Zeeman effect.[45,46]

B. Extension of the Theory

In some experiments[47,48] the electric fields have been so high that second-order perturbation theory is inadequate to predict the correct spectrum. This may also be true in the case of resonance, i.e., where the denominator in Eq. (20) is almost zero. The theory has been extended[44] to the case of high electric fields by finding a general solution of Schrödinger's equation following a method first used by Autler and Townes.[49] In the Hamiltonian of Eq. (19), H_2 is assumed to be of the form

$$H_2(t) = H_2^+ e^{i\omega_0 t} + H_2^- e^{-i\omega_0 t}, \tag{21}$$

where H_2^+ and H_2^- are independent of time. The wavefunction ψ is expanded as

$$\psi(\underline{r},t) = \sum_{m=1}^{M} T_m(t) U_m(\underline{r}). \tag{22}$$

The U_m are the spatial eigenfunctions of the unperturbed atom (assumed known) and $T_m(t)$ are time-dependent coefficients. M is the number of states close to the upper level of the allowed tran-

sition. The T_m are in turn expanded:

$$T_m(t) = e^{-i\lambda t} \sum_{n=-\infty}^{+\infty} C_{mn} e^{-in\omega_0 t}, \tag{23}$$

where λ and the C_{mn} are coefficients to be determined. When (22) and (23) are inserted into (19), the differential equation reduces to an infinite set of linear equations in λ and the C's.

$$(\omega_m - n\omega - \lambda)C_{mn} + \sum_{m'} (\alpha_{mm'} C_{m'n} + \beta^{+}_{mm'} C_{m',n+1} + \beta^{-}_{mm'} C_{m',n-1}) = 0 \tag{24}$$

$$m = 1, 2, \cdots, M; \qquad n = -\infty, \cdots, +\infty$$

$$\alpha_{mm'} \equiv \langle m|H_1|m'\rangle; \qquad \beta^{\pm}_{mm'} \equiv \langle m|H_2^{\pm}|m'\rangle.$$

This set of equations can be solved numerically by truncating the series (23), i.e., assuming $C_{mn} = 0$ for $n > N$ or $n < -N$, where N is determined by the strength of the fields and the accuracy desired (the results of perturbation theory are given by setting $N = 1$). Using the wave function derived from this solution, the spectrum of the light emitted in a transition of the type shown in Fig. 2 has been calculated.[44] In contrast to the results of second-order perturbation theory, in the present case there can be multiple quantum transitions, that is, the atom may emit and/or absorb more than one photon from the external field in going from $i \rightarrow k$. Thus, a whole series of satellites, whose separations are integral multiples of the frequency ω_0, can appear in

the spectrum. These multiple satellites have been observed in an actual experiment.[44] The solution of Eq. (24) also yields the Stark shift of the energy levels of the atom.

C. Use as a Plasma Diagnostic

Using the results of the theories which were outlined above, it is possible to extract detailed information about the electric fields in a plasma from a single set of measurements on the spectrum of light emitted from the plasma. By examining the Zeeman pattern of the satellites and comparing it to theoretical patterns, such as are shown in Fig. 3, the direction of the electric field can be determined. The frequency of the electric field can be found by measuring the separation of the two patterns of satellites, and the amplitude of the fields can be found by measuring the ratio of the amplitude of the satellites to the amplitude of the allowed line and using Eq. (20) or the equivalent one that includes the effect of magnetic fields. The magnitude of the magnetic field can also be determined if it is not previously known by measuring the separation of the Zeeman components of the satellites or the allowed line.

The choice of which spectral line to use when applying the Stark-Zeeman effect is determined by several factors. First, because in most cases the satellites are of low intensity and correspondingly difficult to observe, it is advantageous to choose a strong allowed line that exhibits strong satellites. The intensity ratio S of Eq. (20) can be maximized by choosing ω_{ij} such that the denominator is small, that is, picking an allowed

transition that has a nearly forbidden line. However, for resonance or near resonance when ω_{ij} is very close to ω_0, S may become of the order of, or larger than, unity, in which case the perturbation theory breaks down and the extended theory must be used; in addition it may be difficult to separate the satellite from the allowed line experimentally.

Another consideration in choosing the transition to use is that the matrix elements α and β of Eq. (24) (or R_{ij} in Eq. (20) when it is applicable) must be calculated, which means that the unperturbed wavefunction of the atom must be known. In practice, most of the experimental work has been done using neutral helium lines where hydrogenic wavefunctions can be used; in addition, He I has several strong transitions in the visible where there is a nearby forbidden line. In particular the transitions at 4922 Å ($4^1D - 2^1P$) and 4388 Å ($5^1D - 2^1P$) with the accompanying forbidden lines ($4^1F - 2^1P$) and ($5^1F - 2^1P$) are among the most useful. The triplet lines such as 4472 Å ($4^3D - 2^3P$) are less useful when a magnetic field is present since they exhibit the anomalous Zeeman effect and the Zeeman pattern of the satellites is much more difficult to calculate.

In a plasma the electric field is not usually confined to a single frequency. Perturbation theory gives the result that a distribution in frequency of the electric field will produce a similar distribution in the positions of the satellites.[40] In some cases this may be useful since the frequency spectrum of the fields can be deduced from the optical spectrum; however, if the

frequency spread of the electric field is large, the satellites or their Zeeman pattern may become washed out due to overlapping of the components making up the pattern.

The usefulness of the Stark-Zeeman effect is often limited by the amount of light available, especially for transient plasmas. Unless the electric fields are quite strong (over 1 kV/cm), the satellites usually are weak compared to the allowed line (their intensity, of course, depends upon the particular transition being used and the frequency of the field, as well as the amplitude of the field) and they may be very difficult to resolve over the noise that is present. In this respect it is helpful if the electric field can be switched on and off (in the case of the beam-plasma instability this can be done simply by chopping the beam), since then a differential measurement of the spectrum with and without the satellites can be made.

Another limitation of the technique is that the frequency of the electric field must be quite high or else the satellite patterns will merge into a single pattern centered at the position of the forbidden line. This is further complicated by the fact that the forbidden line is always present in a plasma due to the quasistatic stochastic fields of the ions and/or any static electric fields, due perhaps to macroscopic charge separation. Thus, it may be impossible to separate the effects of these sources of electric field. In practice, if the two satellites are to be separately resolved, the frequency of the electric field must be at least a few GHz, which is a frequency range associated with

plasma electrons, i.e., the electron plasma frequency or the electron cyclotron frequency.

This technique also does not give a spatially resolved measurement of the field as the spectrum is integrated over the volume of plasma defined by the acceptance angle of the optical system. This problem can be mostly overcome when the plasma source is cylindrically symmetric by the technique of Abel inversion (see Appendix C).

Although the use of the Stark-Zeeman effect to measure electric fields does suffer from the difficulties mentioned above, it has the advantage that it provides information about the electric fields in a plasma that may be obtainable in no other way and this information is acquired without perturbing the plasma.

A recent extension of this technique[50] in which the rate of light emission is enhanced by pumping the upper levels of the allowed and/or forbidden transitions by means of a tunable dye laser, enables lower electric field strengths to be measured and permits spatial resolution of the electric fields as well.

IV. EXPERIMENTAL APPARATUS AND PROCEDURE

The following chapter describes the experimental apparatus and procedure used to study the beam-plasma system. The apparatus provided a strong beam-plasma instability which proved suitable for verifying the theory of the high-frequency Stark-Zeeman effect as well as providing information about the beam-plasma system.

A. Apparatus

1. Electron Gun and Plasma Chamber

The arrangement of the electron gun and the plasma chamber is shown in Fig. 4. The electron gun consisted of a resistively heated tantalum filament and two grids. The filament was biased up to 5000 volts negative with respect to ground; the anode, in the shape of a ring, was placed about 10 cm from the filament and was at ground potential. The second grid of the electron gun was held at a constant voltage of +500 volts with respect to the filament. The first grid was used to modulate the electron beam. A square wave of up to 110 volts amplitude (with respect to the filament) could be applied to the first grid by the use of a transistor amplifier operating in the avalanche mode, triggered by a pulse generator. This arrangement provided an electron beam in the plasma chamber of up to 50 mA with a rise time of approximately 10 nsec and a fall time of 100 nsec.

As shown in Fig. 4 the apparatus was divided into three sections with individual vacuum systems: The first two sections were to isolate the electron gun from the high-pressure chamber on the right where the beam-plasma interaction took place. The

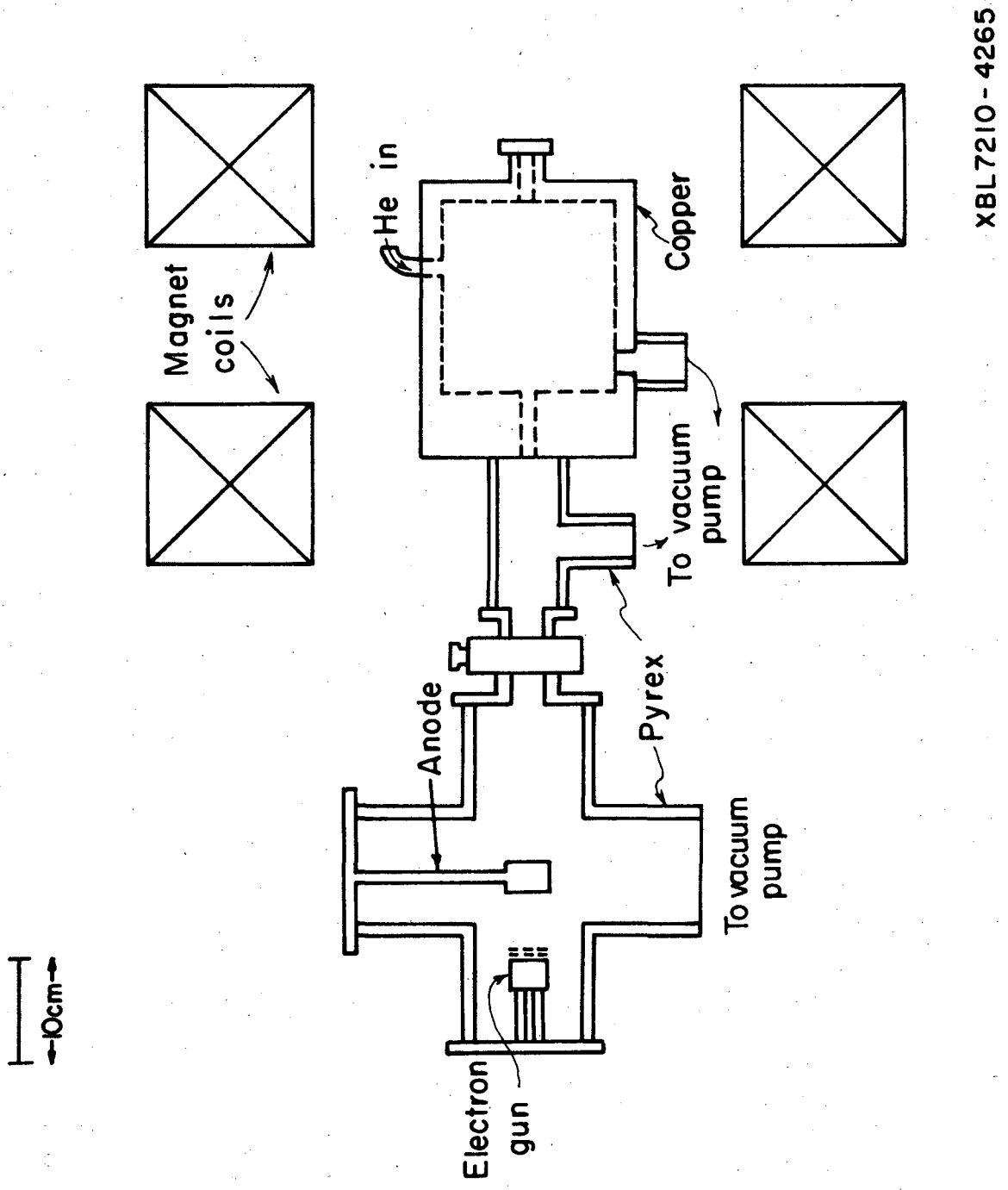

Fig. 4. Diagram of the experimental apparatus.

beam, after passing through the two differentially pumped chambers, entered the third chamber through a small orifice 1 mm in diameter and 5 cm long. The diameter of this orifice determined the diameter of the electron beam inside the plasma chamber.

The plasma chamber was constructed of copper and had an inside diameter of 18 cm and a length of 24 cm. Two ports on opposite sides of the chamber provided access for diagnostic purposes. A copper plate at the end of the chamber, connected to ground through a small resistor, provided a means of monitoring the beam current. There was no provision for suppressing secondary electrons ejected from the copper plate. Helium gas was slowly fed into the chamber by means of a needle valve and the pressure was regulated by adjustment of both the input valve and a valve which controlled the pumpout rate.

The plasma chamber was placed within two magnetic field coils which produced a magnetic field of up to 7600 G along the axis. The coils were arranged nearly in a Helmholtz configuration, and the field strength on the axis was constant to within 1% within the plasma chamber for a distance of 14 cm from where the beam entered the chamber. The fringe fields of the magnets helped to focus and guide the electron beam into the chamber.

2. Optical System

A schematic diagram of the optical system and electronics used for spectroscopic measurements on the plasma is shown in Fig. 5. The light emitted by the plasma was collected by lens 1 and directed to a Fabry-Perot interferometer; the center fringe

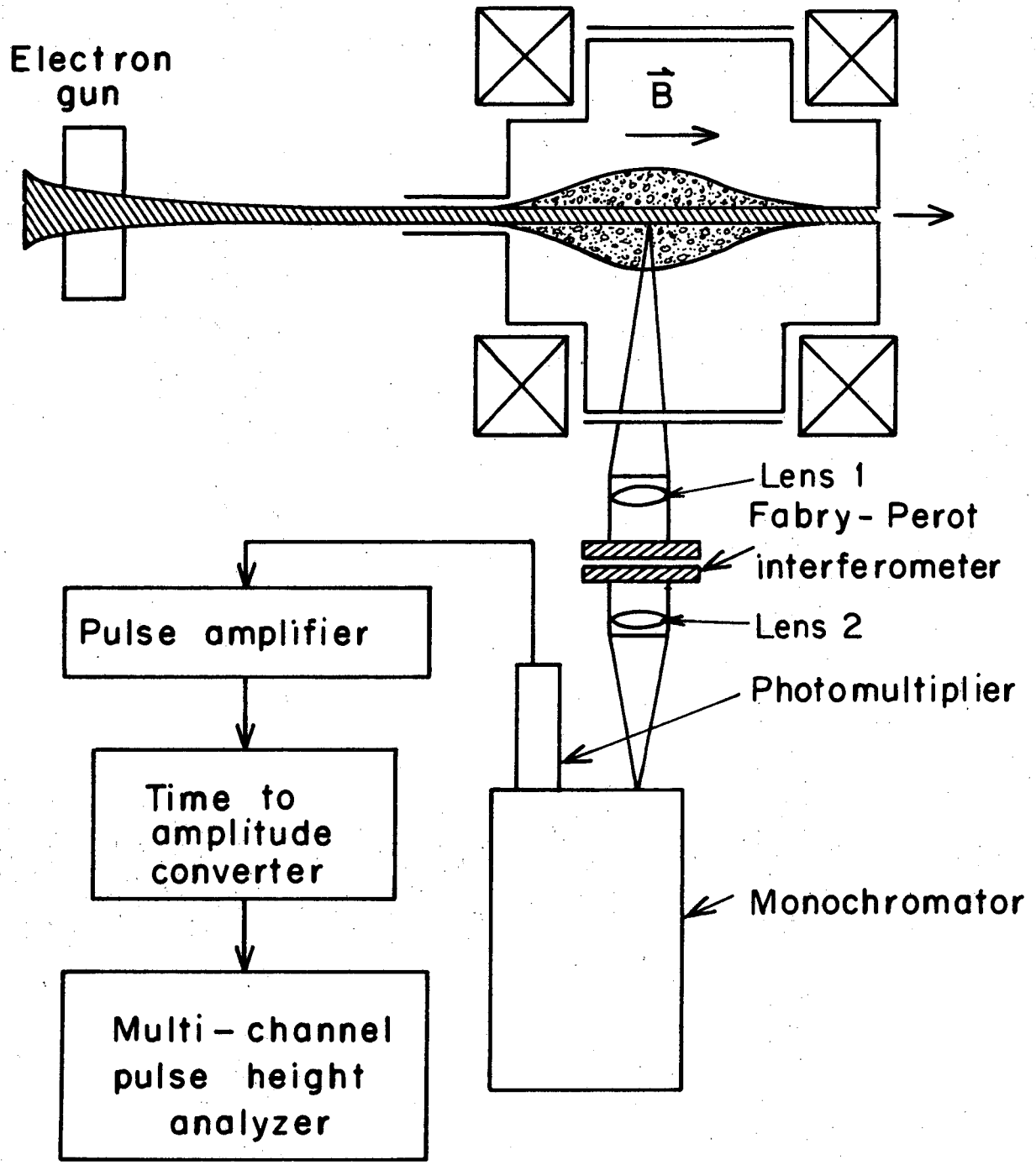

Fig. 5. Schematic diagram of optical and electronic diagnostics.

of the interferometer was focused on the entrance slit of a monochromator by lens 2. The light transmitted through the exit slit of the monochromator was detected by a photomultiplier tube.

Both the interferometer and monochromator were needed in order to provide sufficient spectral resolution to identify the Zeeman pattern of the satellites. The spectral resolution (full width at half maximum) of the system was 0.035 Å. The interferometer was scanned in wavelength by changing the voltage on piezoelectric disks which supported one of its plates. The interferometer, due to its sensitivity to ambient temperature fluctuations, was surrounded by a copper housing whose temperature was regulated by means of circulating water from a temperature-controlled bath.

The spatial resolution of the optical system, given by the size of the image of the entrance slit of the monochromator at the center of the plasma, was 2.66 mm along the beam and 0.076 mm perpendicular to the beam. The system could be scanned horizontally and vertically by moving the optical bench upon which the lenses, interferometer, and monochromator were mounted.

3. Electronics

The electronics used to detect and record the light emitted by the plasma is also shown in Fig. 5. Individual photons were counted for two reasons: First, under some circumstances the intensity of light was very low and statistical fluctuations in the light intensity were the most significant errors in the data; photon counting provided the maximum signal-to-noise ratio. Second, information about the time development of the beam-plasma

instability was desired and photon counting simplified obtaining these data, as explained below.

Pulses from the photomultiplier at the exit slit of the monochromator were amplified by four pulse amplifiers in series. The amplified pulses were input to a descriminator which eliminated weak signals due to noise and produced output pulses of a uniform height and shape. The pulses from the descriminator then went to a time-to-amplitude convertor (TAC). The TAC is simply a device which produces an output pulse whose amplitude is proportional to the time delay between two other pulses, a "start" and a "stop" pulse. A "start" pulse was generated each time the beam was turned on. The "stop" pulse was the amplified pulse from the photomultiplier. Thus each photon detected resulted in an output pulse from the TAC whose amplitude was proportional to the length of time between the turning on of the beam and the time the photon was emitted by the plasma.

The output of the TAC was connected to the input of a multichannel pulse-height analyzer (PHA); therefore, each channel of the PHA recorded photons from a small time interval. By this method a complete picture of the time dependence of the radiation emitted by the plasma was obtained. The data stored in the PHA were punched onto paper tape for processing by digital computer.

The time resolution which was possible with this arrangement was limited by several factors including fluctuations in the transit time of electrons in the photomultiplier, jitter in the rise time of various electronic components, as well as the

linearity of the TAC and PHA. All of these effects limited the resolution to about 20 nsec.

B. Electric Field Measurements

1. Procedure

The spectral line which was most commonly used in the present work for applying the theory of the Stark-Zeeman effect was the 4922 Å (4^1D - 2^1P) line of He I. It was one of the most intense lines emitted by the plasma and the separation of 1.36 Å between the allowed line and the forbidden line (4^1F - 2^1P) was such that, at the observed frequency, the satellite fell conveniently on the wing of the allowed line where it was easily observed. The integrals of the radial eigenfunctions which were needed [as in Eq. (20)] were calculated using hydrogenic wave functions for the excited electron.

Satellites were observed at other lines but these lines were not used for quantitative measurements for a variety of reasons: The spectrum of the 4472 (4^3D - 2^3P) line was complicated by the slight energy differences of the components of the 2P triplet and the fact that it exhibits the anomalous Zeeman effect. The spectrum of the 4388 (5^1D - 2^1P) was also complicated by the fact that its separation from the forbidden line (5^1F - 2^1P) was very close to the frequency of the electric field, and the allowed line and satellite became mixed and difficult to separate.

In these measurements the beam was modulated at a frequency of 500 kHz; the beam was on for 1.5 μsec and off for 0.5 μsec. The modulation of the beam was useful for two purposes: First,

it allowed the investigation of the time development of the beam-plasma instability, and second, it enabled a differential measurement of the spectrum to be made with and without the satellites.

A typical experimental run consisted of a spectral scan at discrete wavelength steps from the peak of the allowed line to the position of the far satellite using the TAC-PHA apparatus to record the temporal behavior of the light emitted. In some cases, only the region where the near satellite was expected to occur was covered, due to the length of time necessary to obtain these spectra. On the wing of the allowed line, where the satellite occurred, the light intensity was very low, and it was necessary to count for a considerable period of time--up to ten minutes--at each wavelength point in order to gather enough counts, about 1000 counts/channel, to provide the statistics desired. The spectrum was usually made in steps of 0.05 Å and a complete run would sometimes take 6 hours or more. The data were reproducible over periods of this length of time, and as a rough measure of how steady the plasma was, the peak intensity of the allowed line did not change more than 5% during a run in most cases.

In order to determine the electric field as a function of radius, a vertical scan (that is, perpendicular to the beam axis) was made at each wavelength desired and Abel inversion (see Appendix C) was used to determine the local emissivity of the plasma. Since this was also a time consuming process, usually just points at the peak of the allowed line and the peak of the satellite were Abel inverted.

2. Typical Results and Analysis of Data

Figure 6 shows the temporal behavior of the light at a wavelength of $\Delta\lambda = -0.80$ Å from the peak of the 4922 Å line observed during a typical experimental run. The abscissa is the channel number of the PHA and the ordinate is the number of photons collected per channel. One satellite occurs near $\Delta\lambda = -0.80$ Å and it is seen that the intensity drops off rapidly when the beam is turned off. The light that remains after the electric field has vanished is from the wing of the allowed line, continuum radiation, and dark current of the photomultiplier.

Figure 7 shows complete spectra near 4922 Å of light emitted during beam-on and beam-off time intervals. The direction of observation is perpendicular to the magnetic field and the direction of polarization of the emitted photon is parallel to the magnetic field. The double arrows indicate peaks in the spectrum due to orders of the interferometer; they are purely instrumental. The single arrow indicates where the forbidden line occurs at $\Delta\lambda = -1.36$ Å.

As can be seen in Fig. 7, the beam-on and beam-off spectra are nearly identical except in the regions $-1.0 \lesssim \Delta\lambda \lesssim -0.6$ and $-2.2 \lesssim \Delta\lambda \lesssim -1.8$; these regions are where the two satellites occur. The two spectra are otherwise similar since the density of the plasma, which is what mainly determines the shape of the wing of the allowed line, did not change very much during the 0.5 μsec that the beam was off. However, the overall intensity of the line did begin to drop and the amplitude of the electric field

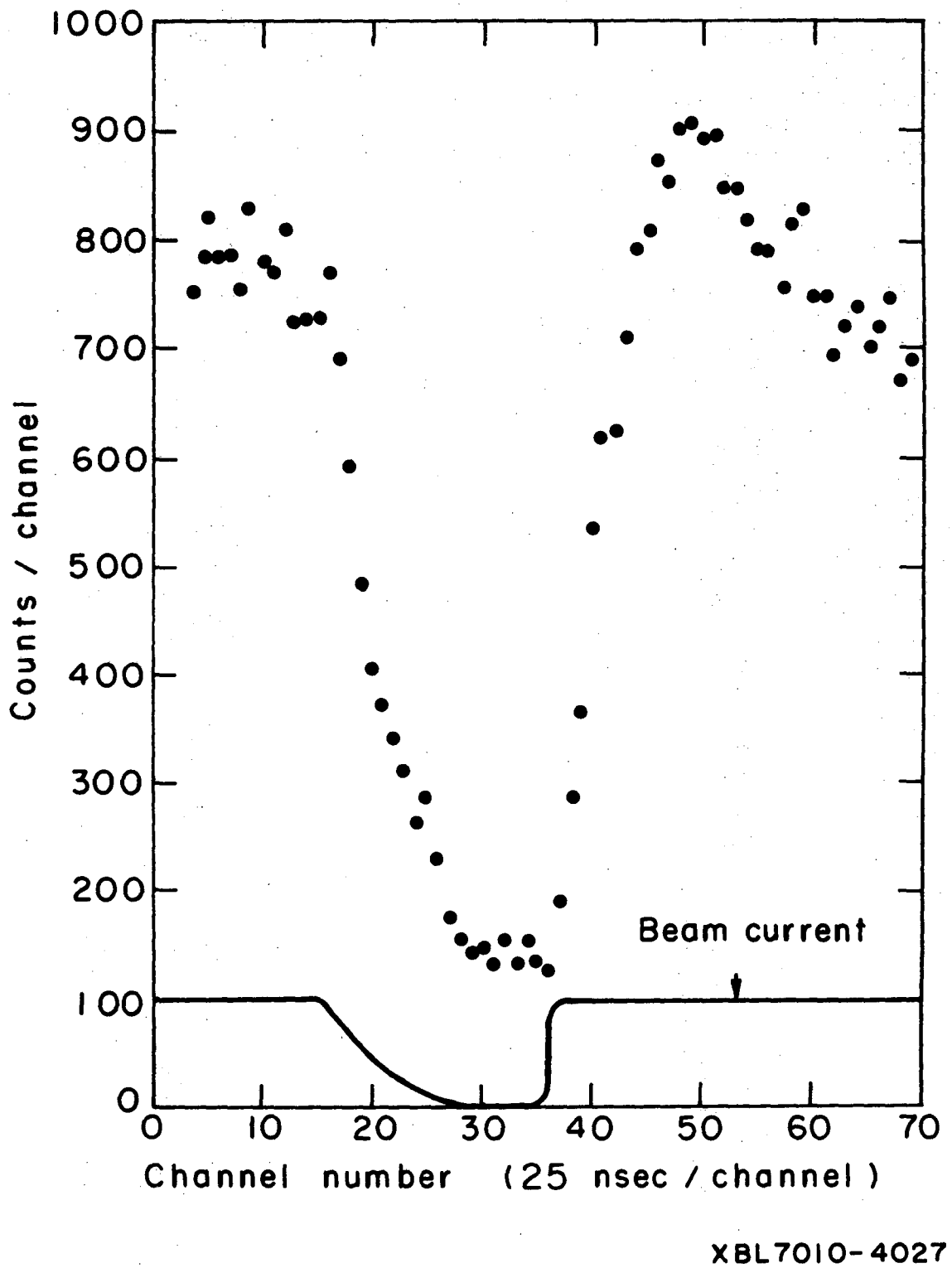

Fig. 6. Typical result for a single spectral point showing time dependence of light emitted. Ordinate is proportional to light intensity. Beam current is shown superimposed with same time scale.

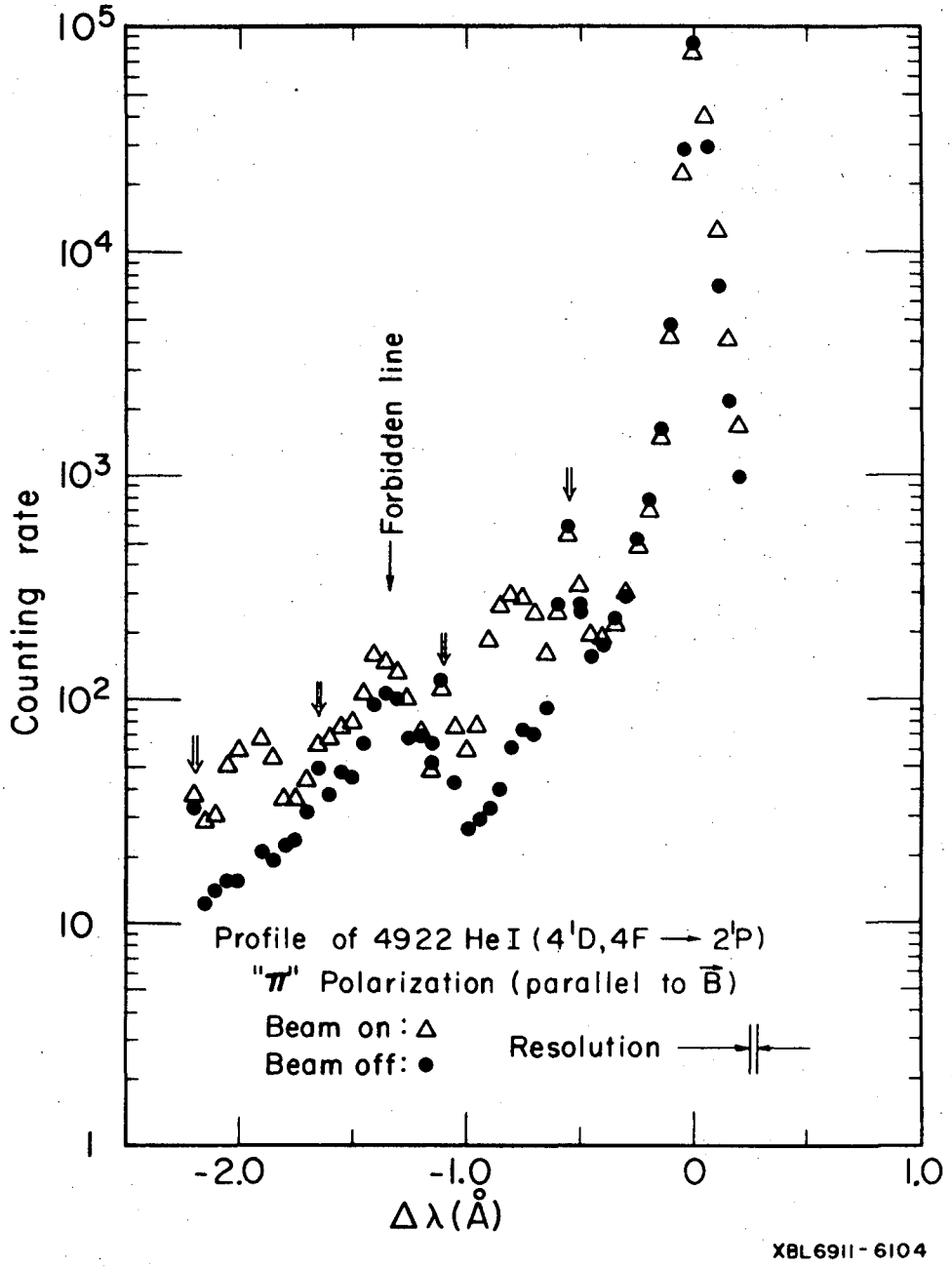

Fig. 7. Complete spectra during beam-on and beam-off time intervals. Double arrows indicate where orders of the interferometer fall.

decreased significantly while the beam was off. The beam-off spectra show only a very small bump in the regions where the satellites occurred, indicating that the electric field had nearly completely died away during the time that the beam was off.

This similarity between the beam-on and beam-off spectra was used in analyzing the data; the beam-off spectrum was multiplied by a constant factor to take into account the overall decrease in the line intensity and then subtracted from the beam-on spectrum; the resultant spectrum clearly showed the satellites. A channel or group of channels which occurred just before the beam was turned on was used as the beam-off spectrum. The "beam-on" spectrum was any other channel. By measuring the satellites as a function of time in this way the temporal behavior of the electric fields was determined.

V. RESULTS AND DISCUSSION

The results of measurements made on the beam-plasma system using the apparatus and procedures described in Ch. IV are given below. Included is a general, mostly qualitative, description of the beam-plasma as well as more specific results concerning the electric fields in the plasma and other plasma properties. The consistency of the various results is examined, and, where possible, compared with theory. Some preliminary results of this experiment have already been published by Cooper and Hess.[43]

A. Qualitative Observations

A series of photographs of the beam-generated plasma is shown in Fig. 8. The direction of beam flow is from left to right in the photographs. The electron beam, which followed the magnetic field lines along the axis of the plasma chamber, formed a narrow cylinder of plasma with a constant diameter of approximately 1 mm. This plasma cylinder was surrounded by a luminous "halo" of plasma whose radius and brightness varied along the beam direction. The halo had a peak luminoisty not on the beam axis, but at a radius of about 2 mm.

One of the most distinctive features of the plasma was its tendency to exist in discrete "modes". These modes were observable visually and were characterized by the size, position, and brightness of the plasma; a few of these modes are shown in Fig. 8. Which mode was excited depended most sensitively upon the beam current; as the beam current was increased, the plasma would jump from one mode to another, moving closer to the point where

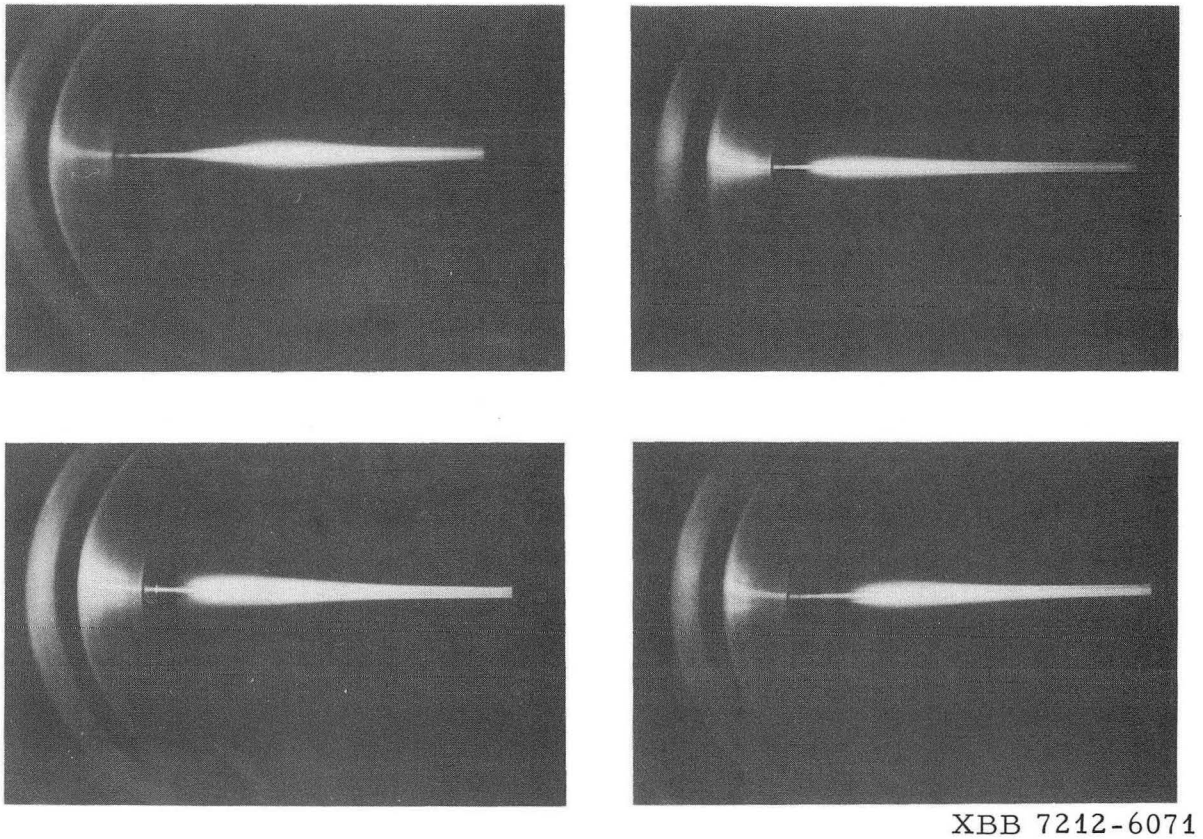

XBB 7212-6071

Fig. 8. Photographs of beam-generated plasma showing four different "modes". Direction of beam flow is from left to right. Exposure: 1/15 sec at f8 on Tri-X.

the beam entered the chamber and simultaneously increasing in size and brightness. Three or four of these modes were observable as the beam current was increased to its maximum value. As mentioned in Ch. III, Seidl and Sunka[21] observed the density in their beam-plasma system assumed values such that $\omega_H = (\omega_p^2 + \omega_c^2)^{1/2} = m\omega_c$, where m is an integer. The modes observed in the present experiment may have been similar to theirs, although in their experiment the neutral gas pressure was much lower (10^{-3} to 10^{-5} Torr). Moreover, the determination of the density in the present experiment was not accurate enough for a quantitative test of the above expression.

The intensity of the light emitted by the plasma varied axially, that is in the direction of the beam, and most of the measurements performed on the plasma were made at the axial position where the intensity of the light was greatest. This maximum was found to occur at a distance of 2 to 4 cm from where the beam entered the chamber, depending upon the beam parameters and the "mode". The point of maximum light emission was found to be the same for different spectral lines, such as the 4922 Å and 4388 Å He I lines.

The response of the beam-plasma to a change in the magnetic field alone was difficult to obtain since the magnetic field also focused and guided the electron beam and a change in the magnetic field led to a change in some of the properties of the beam as well. As the magnetic field was varied from 5 to 7.5 kG, no radical change was observed in the nature of the plasma, but the

plasma would usually jump from one mode to another.

The beam-plasma was not sensitive to small changes in the neutral gas pressure, but the plasma did change in appearance rather suddenly if the pressure was raised above ~ 1.0 Torr or lowered to below ~ 0.03 Torr. In both cases the plasma became uniform in radius and luminosity along the beam direction, and the "mode" behavior was absent. Although a beam-plasma instability may have been present in the cases of high and low pressure, the intensity of the light that was emitted was insufficient to allow the use of the Stark-Zeeman effect to measure the electric fields.

B. Beam Parameters

The beam parameters are listed in Table I. The beam current was determined by measuring the current striking the plate at the end of the plasma chamber with the neutral gas pumped out. The parameters listed apply to the beam when it was completely turned on. When the voltage of the grid of the electron gun was biased negative in order to turn the beam off, a small amount of beam current--approximately 1 or 2 mA--was still present. The energy density that is given in Table I is the energy of directed motion ($1/2\ mu^2$) in the laboratory frame. Although it was not measured, the width of the beam distribution function was estimated to be not more than a few electron volts.

C. Plasma Parameters

The plasma parameters of most importance, namely the plasma density and the electron and ion temperature, were more difficult to determine than the beam parameters, especially since they were

Table I. Electron beam parameters.

Energy	4	keV
Velocity	3.75×10^{9}	cm/sec
Current	4.0×10^{-2}	A
Current density	5.1	A/cm^2
Energy density	54	$ergs/cm^3$
Electron density	8.5×10^{9}	cm^{-3}
Diameter	0.10	cm

strong functions of position, both axially and radially, and the results for the temperatures are no more than estimates.

1. Density

Langmuir probes were used to measure the local density of the plasma from a distance of several mm to 1.4 mm from the beam axis. The probes could not be used nearer to the beam axis since the power in the beam was sufficient to destroy them. The density of the plasma was calculated from the ion saturation region of the curves, using the method of Sonin.[51]

The density was also found by measuring the intensity ratio of the forbidden line $4^1F - 2^1P$ of He I to the allowed line $4^1D - 2^1P$ (see Appendix D). The density was determined by using Eq. (D3) and Abel-inverted data for the intensity of the allowed and forbidden lines. The results of these measurements, as well as the results of the data collected with the probes, are shown in Fig. 9. The points marked with dots are the spectroscopic measurements while the points marked with triangles are the probe data. The spectroscopic data did not extend beyond a radius of 2.3 mm as the intensity of the forbidden line was so low that it was difficult to separate from the noise present. For reasons given in Appendix D the spectroscopic results are uncertain by a constant factor of $\lesssim 2$ and, moreoever, there is uncertainty in the relative values for the density near the center of the beam. The error in the probe measurements was estimated to be ±50%, primarily due to the magnetic field present.

The results of measurement of the plasma density given above

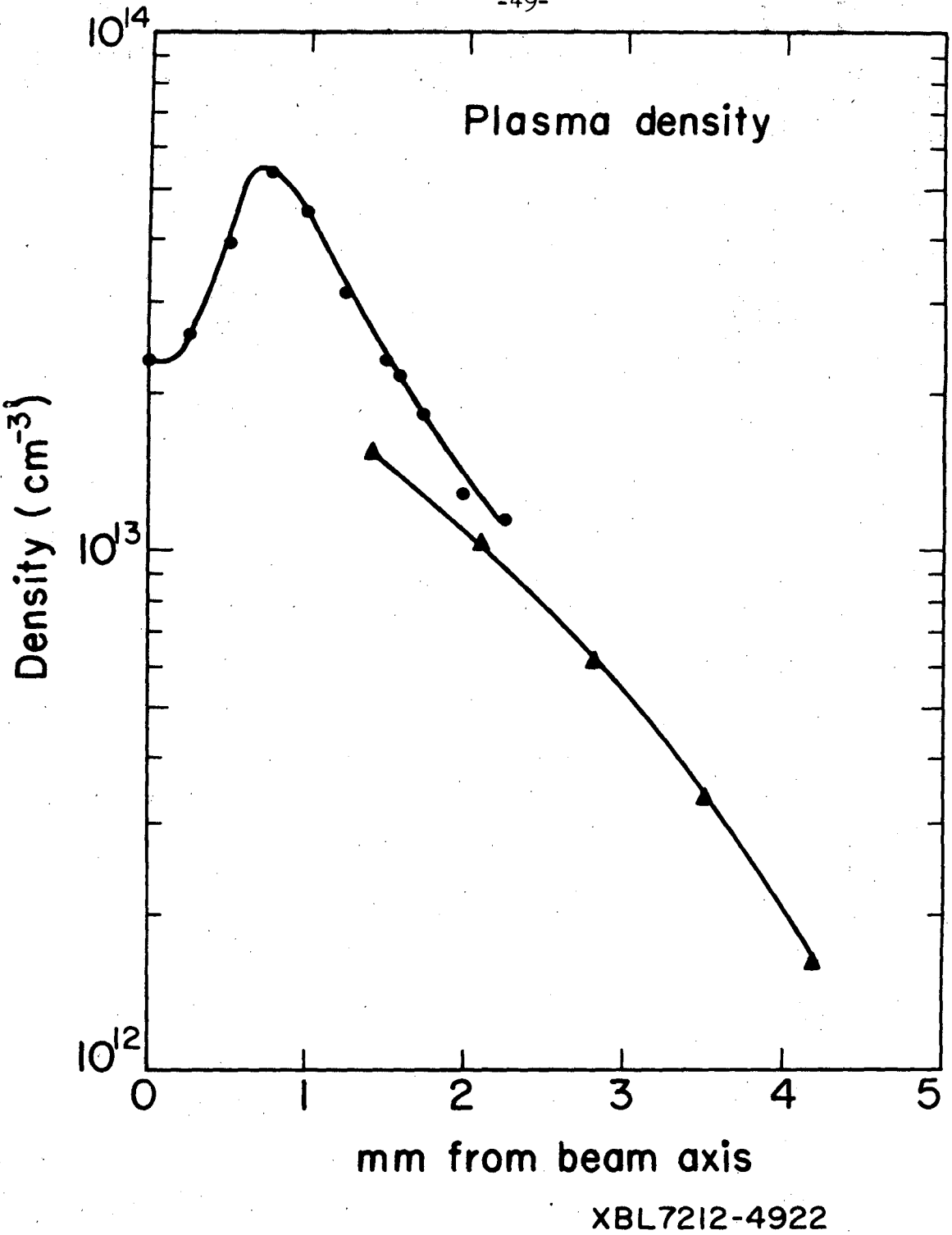

Fig. 9. Ion density of beam-generated plasma. Dots indicate results of spectroscopic measurements. Triangles indicate data using Langmuir probes.

agree within errors with results found by measurement of the broadening of the 4922 Å He I line.[52]

2. Electron and Ion Temperatures

The ion temperature was estimated by measuring the width of the 4686 Å He II line. For the densities observed in the present experiment, Doppler broadening is the main contribution to the half-width of the line for temperatures above 100 K. Unfortunately, the measurement of the half-width of the line is complicated by the fine-structure of the ionized helium line, the 4686 line being split into two main components of about equal intensity, separated by 0.11 Å. Taking into account the line splitting as well as the instrumental broadening, the temperature of the ions was estimated to be less than 0.15 eV.

The electron temperature was also estimated from observations made on the 4686 He II line; the intensity of this line for a beam-on time of 10 μsec and a beam-off time of 9 μsec is shown in Fig. 10. These data were taken on the beam axis with no Abel inversion, but Abel inversion at selected time intervals showed very similar results for points within the beam radius. After the beam is turned off the light emitted initially decreases but then rises to a sharp peak after 5 μsec. The peak is due to recombination light, that is, light emitted as He III recombines with electrons to form He II. Some of the recombination is into excited states of the He II ion, which then cascade downwards toward the ground state, producing lines such as the 4686 line, which is a $n = 4 \rightarrow 3$ transition.

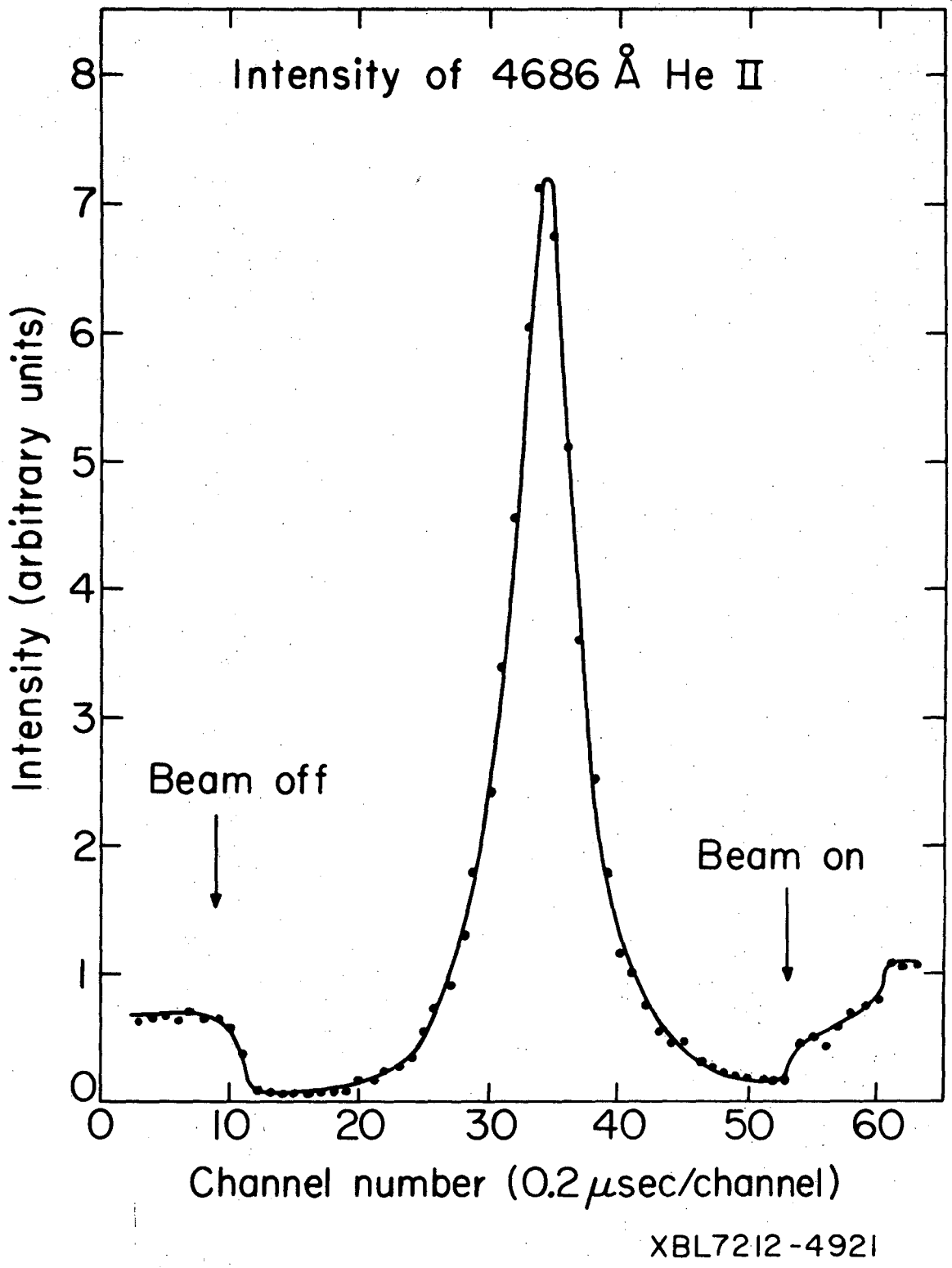

Fig. 10. Intensity of the 4686 He II line as a function of time.

The time delay between the turning off of the beam and the peak in the recombination light is due to the strong temperature dependence of the recombination rate; for $T_e \gtrsim 1$ eV, the recombination rate is proportional to $T_e^{-3/4}$ and for $T_e < 1$ eV, it increases very rapidly with decreasing temperature.[53] The recombination rate will begin to decrease again when the population of He III is depleted by the recombination or by diffusion of the ions from the region of the beam.

From considerations of the intensity of the recombination light it seems reasonable to assume that the ratio of the density of He III to He II was between 10^{-2} to 10^{+2}. If the ratio was much less than 10^{-2}, the large intensity of the recombination light would be difficult to explain, and if the ratio was greater than 10^{2}, the intensity of the 4686 line when the beam is on would be much less than is observed.

Applying the theory of Elwert[54] to calculate what the ratio should be for various electron temperatures, the result is that for the above limits on the ratio of He III to He II, the electron temperature is in the range $4.4 \text{ eV} \lesssim T_e \lesssim 22 \text{ eV}$.

D. Electric Fields

The electric fields due to the beam-plasma instability were investigated using the procedure given in Ch. IV and the theory of the Stark-Zeeman effect given in Ch. III. The satellites were usually measured at the axial position where the allowed line was most intense. The electric fields were found to be of maximum intensity at the same position and this facilitated the quanti-

tative measurement of the satellites since both their intensity relative to the allowed line and their absolute intensity were greater. This meant that the satellites were more easily seen above the noise present in the spectrum due to fluctuations in the plasma, statistical fluctuations in the light emitted, and the dark current of the photomultiplier.

Results are given in Sects. 1 and 2 below for the measurements of the polarization, frequency, and amplitude of the electric fields. The results were obtained by comparison of experimental spectra with theoretical calculations. The extended theory as given in Sect. B of Ch. III was used although for the frequencies and electric field strengths found in the present experiment, perturbation theory was adequate.

1. Amplitude

The amplitude of the electric field was determined by measuring the ratio of the intensity of the satellites to the intensity of the allowed line. Data were taken at a number of radial points to allow Abel inversion of the respective intensities. Figure 11 shows the Abel-inverted data of the light emitted at 0.0 Å and -0.80 Å from the center of the 4922 Å line. The various curves represent the radial dependence of the intensity for different times after the beam was turned on. The electron beam was on for 1.5 μsec and off for 0.5 μsec for the data shown in Fig. 11 and for the rest of the data given in this chapter. In each case the lowest curve corresponds to light emitted in the time interval (25 nsec) during which the electron beam was turned on. The

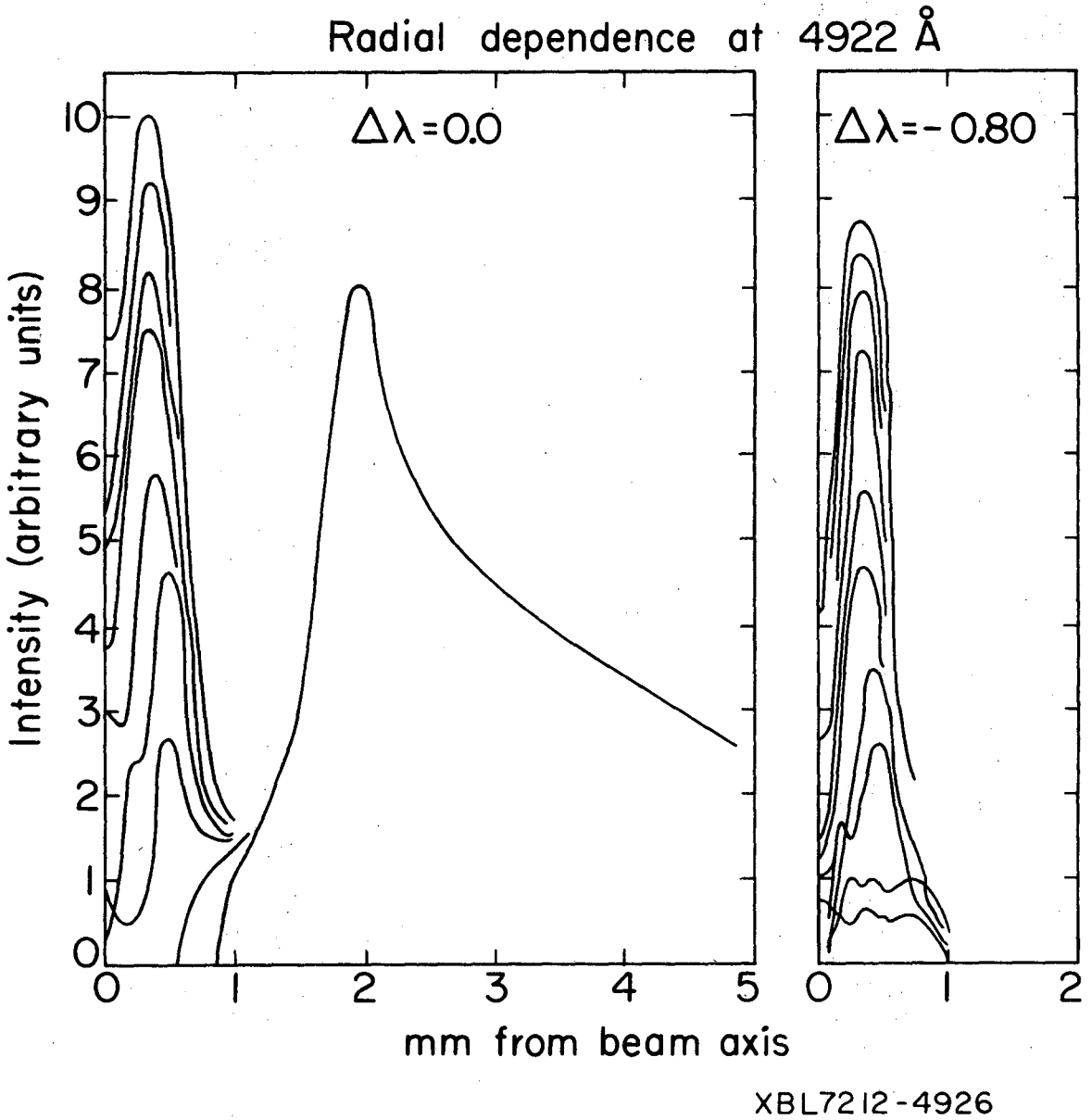

Fig. 11. Abel inverted radial dependence of the light emitted at 0.0 Å and -0.80 Å from the peak of the 4922 Å He I line. The lowest curves are due to light emitted just before the electron beam is turned on. Progressively rising curves show the intensity of the light emitted during successive 25 nsec time intervals.

progressively rising curves are the light emitted during successive 25 nsec intervals. The light emitted at $\Delta\lambda = 0.0$ within a radius of 1 mm is low when the beam is off but rises rapidly when the beam is turned on. However, the light from the region beyond 1 mm is practically constant in intensity and does not change significantly during the 0.5 μsec that the beam is off. For the particular experimental run from which the data of Fig. 11 was taken, $\Delta\lambda = -0.80$ was close to the peak of the near satellite. The light emitted at $\Delta\lambda = -0.80$, and hence the electric field of the instability, was nearly confined to within the radius of the beam, and had very little intensity when the beam was off. Both the light emitted at $\Delta\lambda = 0.0$ and $\Delta\lambda = -0.80$ had their maximum intensities not on the axis of the beam but somewhat inside the edge of the beam (radius 0.5 mm). Although the error in the Abel inversion increases towards the center, it is believed that the dip in the center is real; a similar dip in the ion density of the plasma can be seen in Fig. 9.

The amplitude of the electric field at the edge of the beam is shown in Fig. 12 as a function of time. The beam was turned on during Channel 37 and Fig. 12 shows that by Channel 38 (25 nsec after beam turn-on) the electric field is not growing exponentially but is near to its saturation value.

The electric field is shown as a function of radius in Fig. 13. In this case, the data from a number of channels corresponding to times after the electric field had saturated have been added together to increase the accuracy of the results.

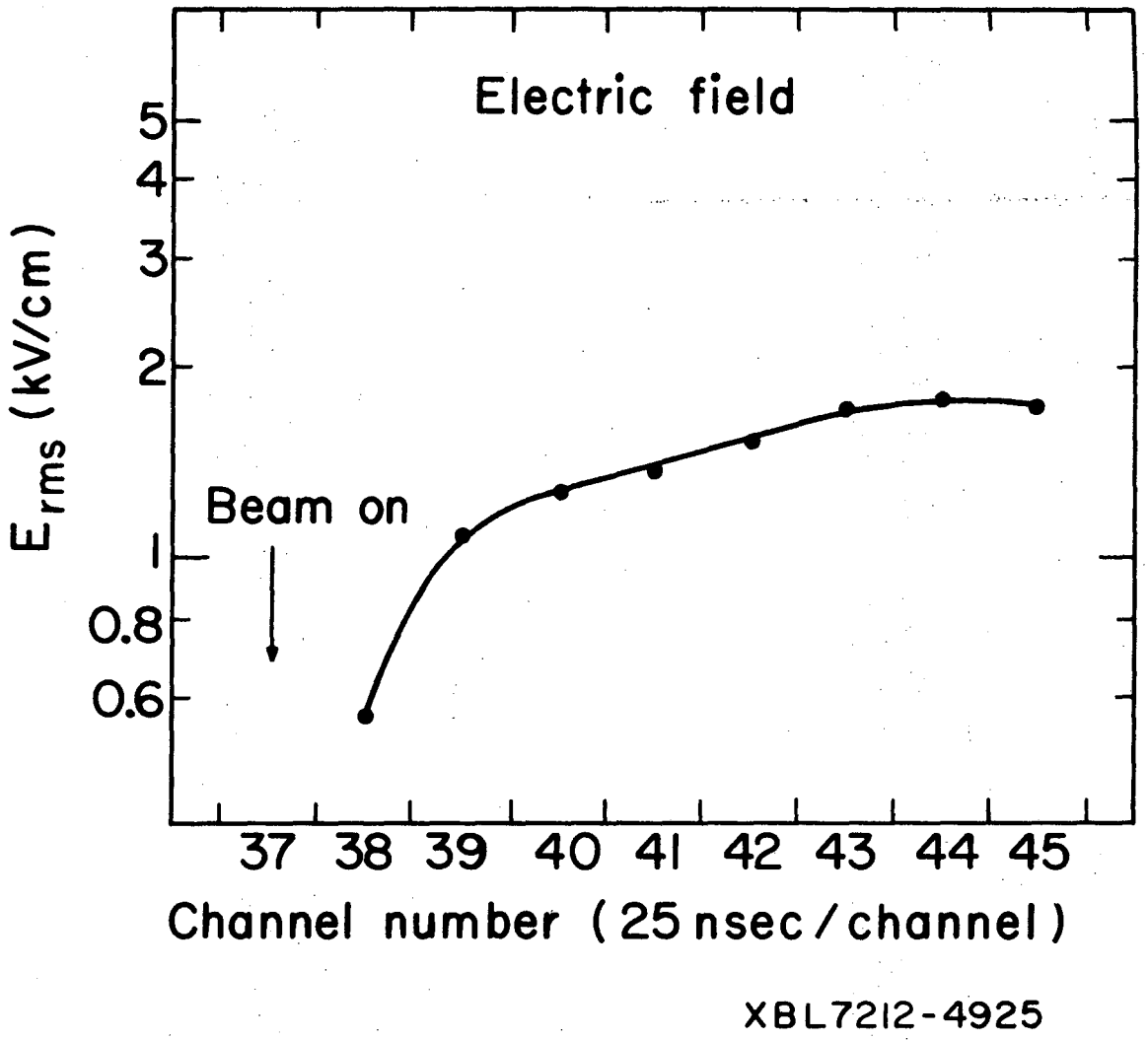

Fig. 12. Time dependence of electric field strength.

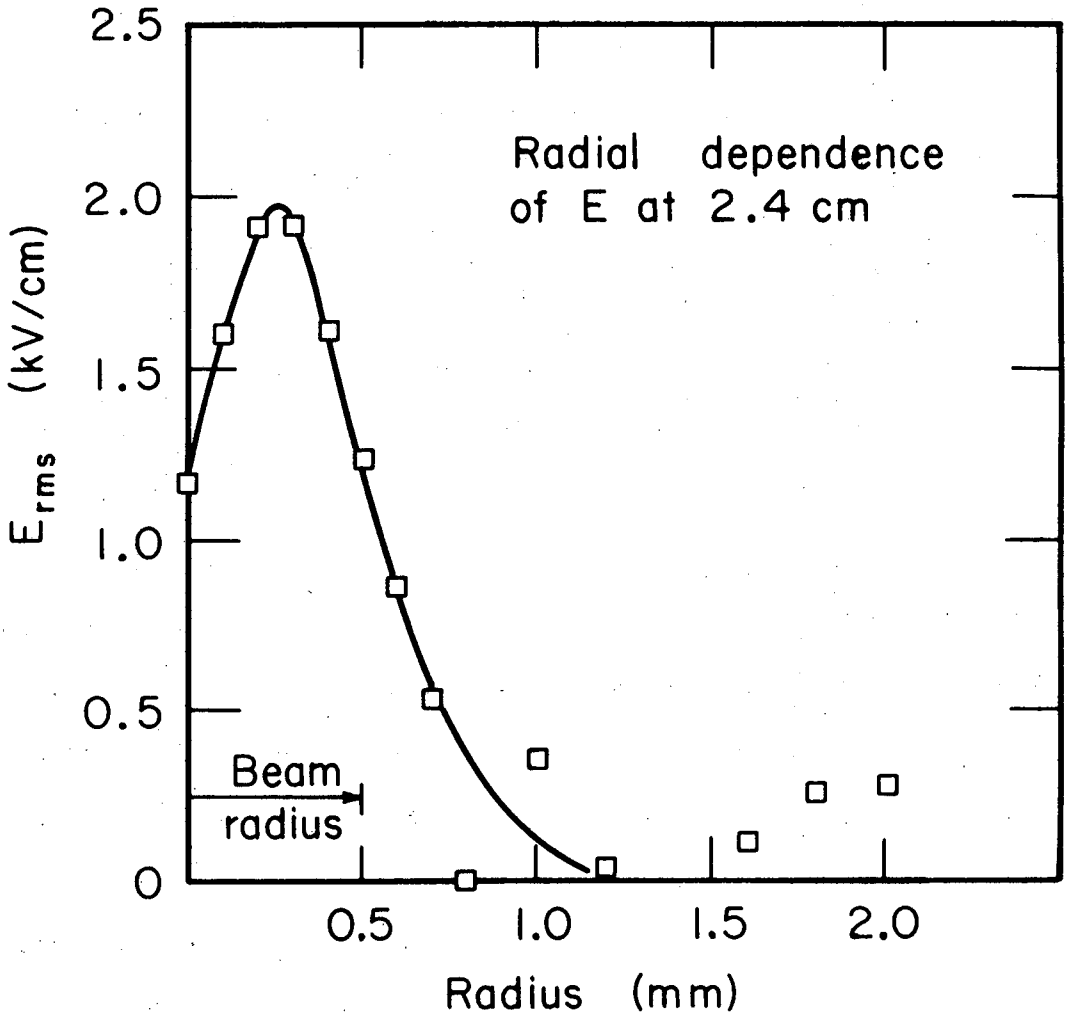

XBL 6911-6121

Fig. 13. Abel inverted radial dependence of the electric field strength at a time after the field had saturated. Data were taken at a distance of 2.4 cm from where the beam enters the plasma chamber.

These data were taken at a distance of 2.4 cm from where the beam enters the chamber. Here again, there is a dip in the center of the beam, and the electric field is confined mainly to the edge of the beam. The points beyond 1.55 mm, which show a rise in the electric field are not valid but are due to errors in the original data and the effects of the Abel inversion.

The amplitude of the electric field is shown in Fig. 14 as a function of the distance from where the beam enters the plasma chamber. The electric field also decreased rapidly at distances beyond the peak at 2.1 cm. The dashed line in Fig. 14 corresponds to an e-folding distance for the electric field of 1.8 cm.

2. Polarization and Frequency

The polarization and frequency were found by comparing experimental and theoretical Zeeman patterns. Figure 15, taken from Ref. 43, shows the region of the spectrum near the 4922 He I line where the two satellites and the forbidden line occurred. A Zeeman pattern computed theoretically is shown as vertical lines superimposed on the experimental results. For a direct comparison of theory and experiment, the theoretical curves would have to be folded with the instrument profile and the (unknown) line profile. The theoretical pattern was calculated assuming that the electric field was linearly polarized and random in direction. The frequency chosen, which gave the best fit to the experimental pattern, was 74.4 GHz. The forbidden line, which occurs at the center of the two satellites near $\Delta\lambda = -1.35$ Å, is seen to also have a Zeeman pattern indicating an electric field

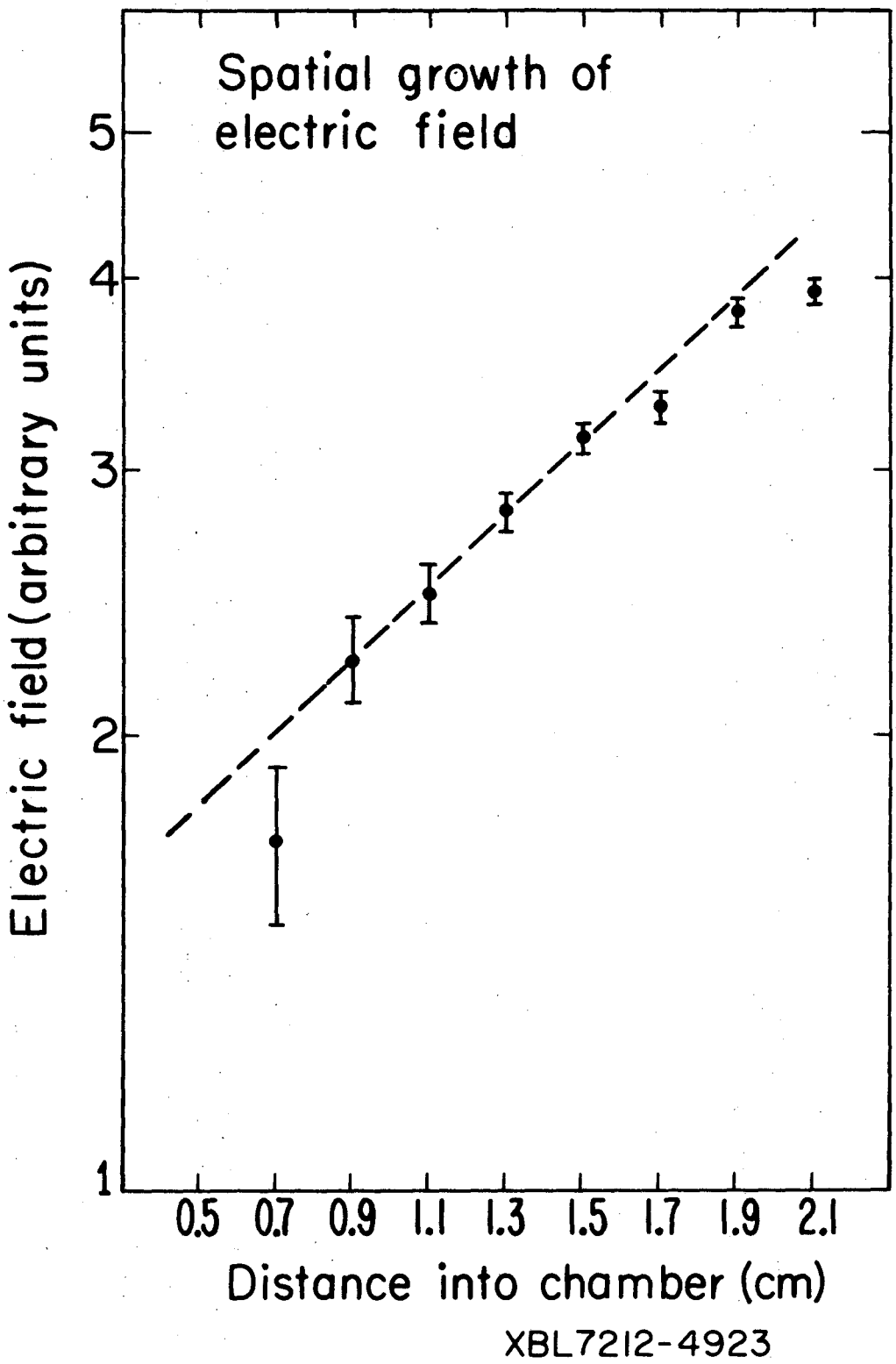

Fig. 14. Spatial growth of the electric field at a time after which the electric field had saturated.

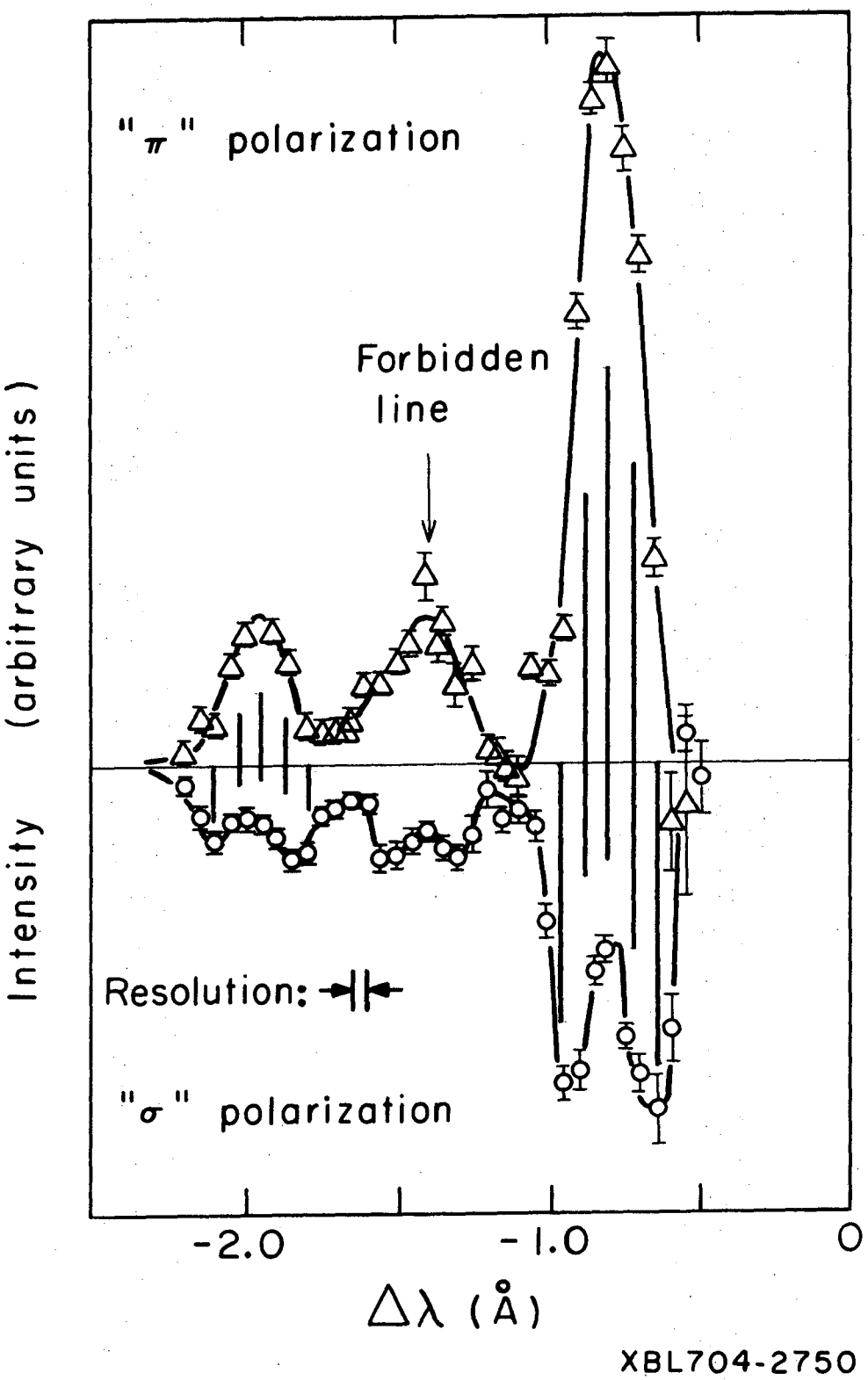

Fig. 15. Measured (triangles and circles) and calculated (vertical solid lines) spectra due to beam-generated plasma. $\Delta\lambda$ is the separation from the center of the allowed 4922 Å He I line.

random in direction which is to be expected since the forbidden line is due to the stochastic fields of the ions. In Fig. 15 and the rest of the results for this subsection, the spectra have not been Abel inverted, so the spectrum that is observed is one spatially averaged over the volume where the fields occur. However, this spatial averaging should have have a strong effect on the shape of the Zeeman patterns since practically no light is emitted at the wavelength of the satellites from the region where there is no electric field. Because of this averaging over regions where the field strength had different values, the theoretical patterns were calculated for an electric field of 1 kV/cm, rather than the peak field of ~ 2 kV/cm.

Figures 16 and 17 show the time behavior of π and σ components of the near satellite for a different experimental run. Again the successively increasing curves represent successive channels (with 25 nsec) beginning immediately after the beam is turned on. The Zeeman splitting for the magnetic field present in this case (6440 G) is shown at the figure, indicated by the symbol λ_L. Figure 18 shows a comparison between the experimental and theoretical results; the experimental spectrum was found by adding together a number of channels which corresponded to times after the electric field had saturated in order to reduce the errors due to fluctuations. The theoretical pattern was calculated assuming an electric field of 1 kV/cm, a frequency of 74.4 GHz, and an electric field random in direction.

The experimental results of Figs 16-18 can be compared with

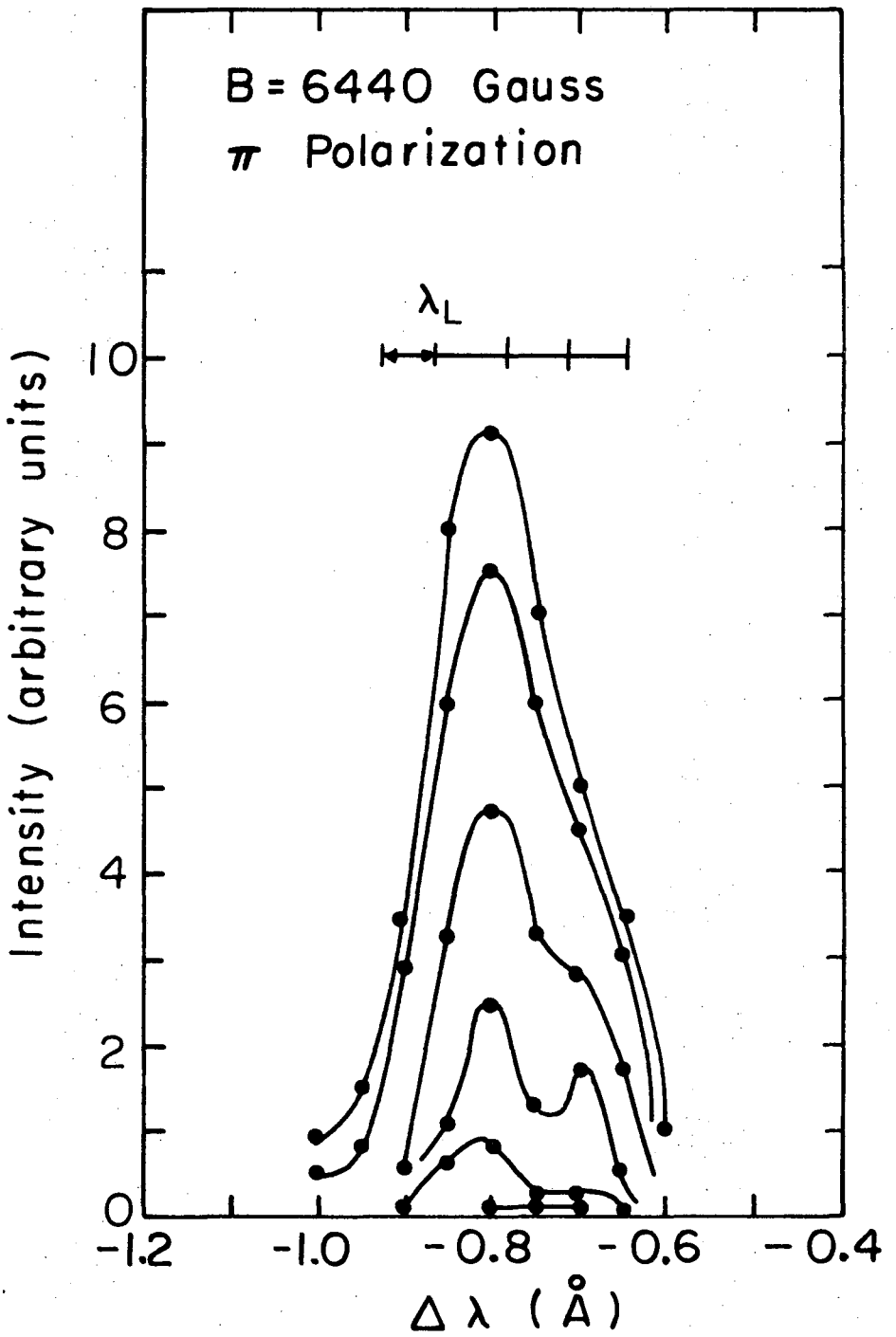

XBL7210-4271

Fig. 16. Near satellite of 4922 Å He I line. Successive curves are spectra integrated over successive 25 nsec time intervals. Curve at bottom was simultaneous with turning-on of the beam. λ_L indicates Larmor splitting. π polarization is shown.

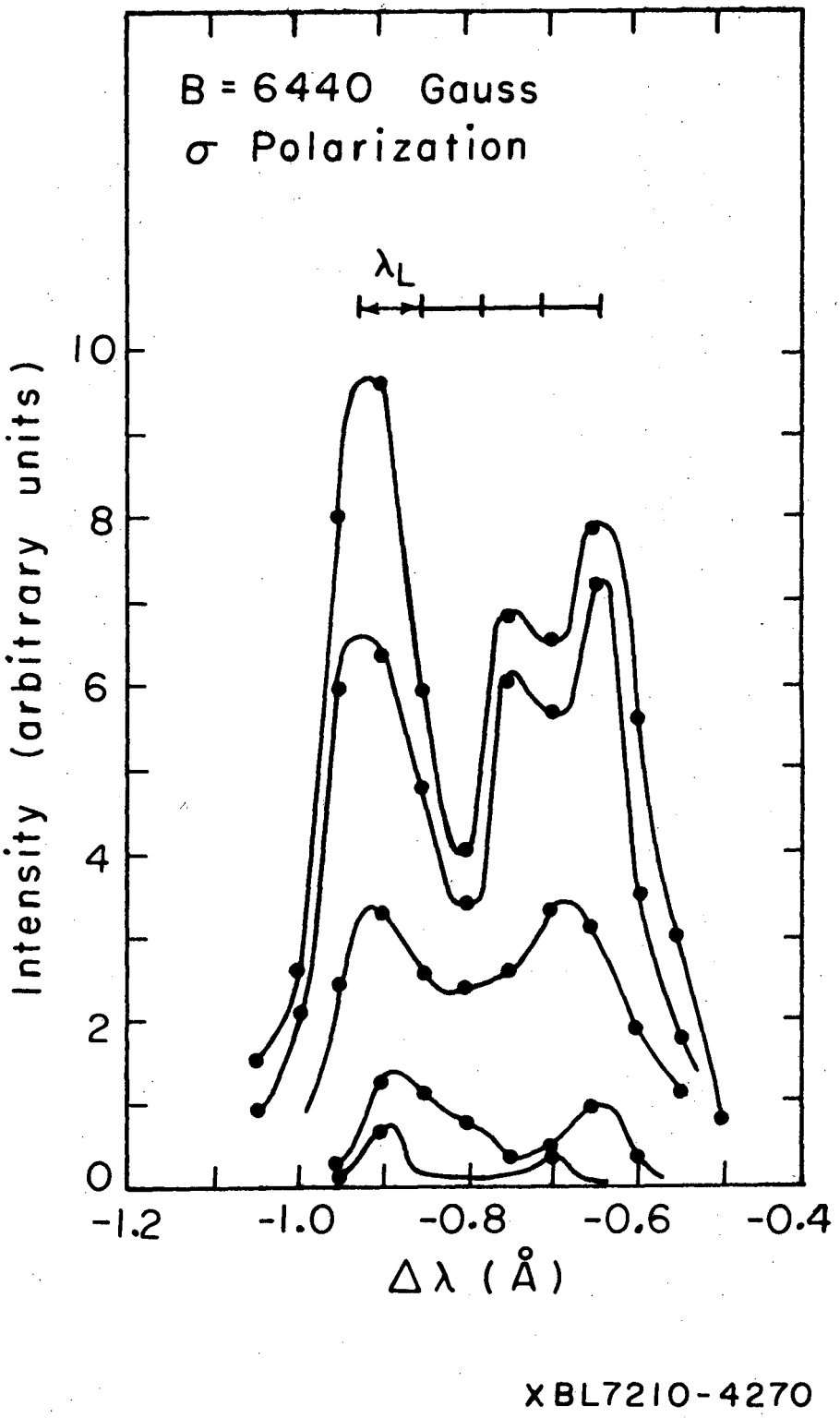

Fig. 17. Same as Fig. 16 except σ polarization is shown.

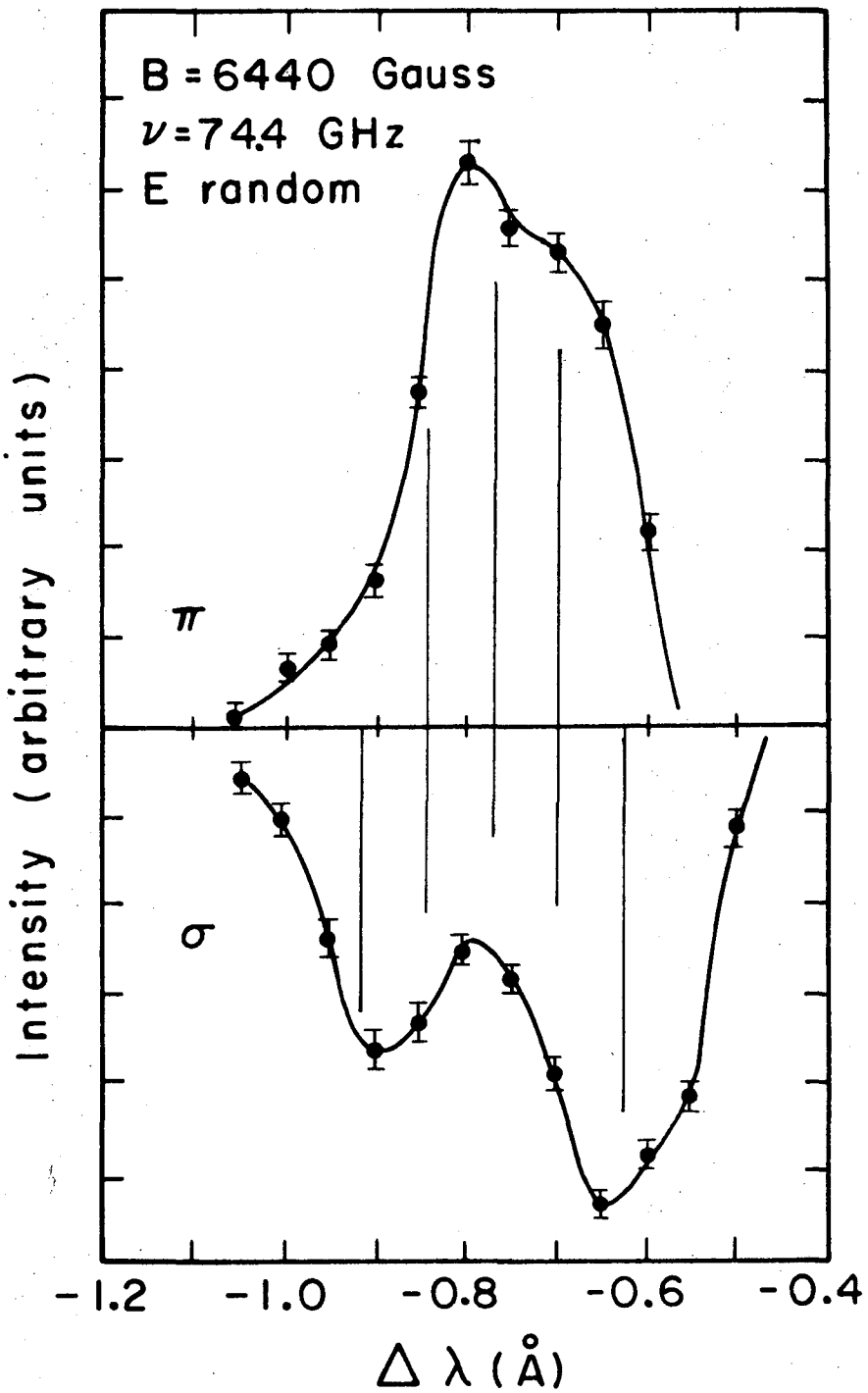

XBL7210-4266

Fig. 18. Same data as Figs. 16 and 17 but showing spectrum after electric field had saturated. Dots are experimental points. Vertical bars are results of theoretical calculations for indicated frequency and magnetic field, and for an electric field random in direction.

the results of another experimental run, this time at a magnetic field of 7580 G and slightly different beam parameters, shown in Figs. 19-21. Figures 19 and 20 show the time development, while Fig. 21 is a comparison with theory of the spectrum due to the saturated electric field. In Fig. 21, the theoretical spectrum was calculated assuming an electric field of 1 kV/cm, a frequency of 73.2 GHz, and an electric field which was perpendicular to the magnetic field and random in azimuthal angle. The difference between the polarization patterns of Figs. 18 and 21 is quite noticeable, particularly the dip in the center of the π pattern in Fig. 21, while Fig. 18 has a peak at the same wavelength. The difference between the two patterns is not due to the difference in the magnetic field, since Zeeman patterns similar to Fig. 18 were observed at a magnetic field of 7580 G also. Both "modes" could be reproduced but the mode with $\vec{E}$ random was normally the one present. The mode with $\vec{E} \perp \vec{B}$ was obtained only by trial-and-error by making small changes in the beam parameters (which would cause the plasma to jump from one mode to another) until a Zeeman pattern similar to that in Fig. 21 was seen. There were no visually observable characteristics of the plasma that indicated which of the two polarizations was present.

E. Discussion of Results

1. Plasma

Table II lists some of the basic plasma parameters. The cyclotron frequencies were calculated for B = 7000 G and the collision frequencies were calculated assuming $n_e = 5 \times 10^{13}$,

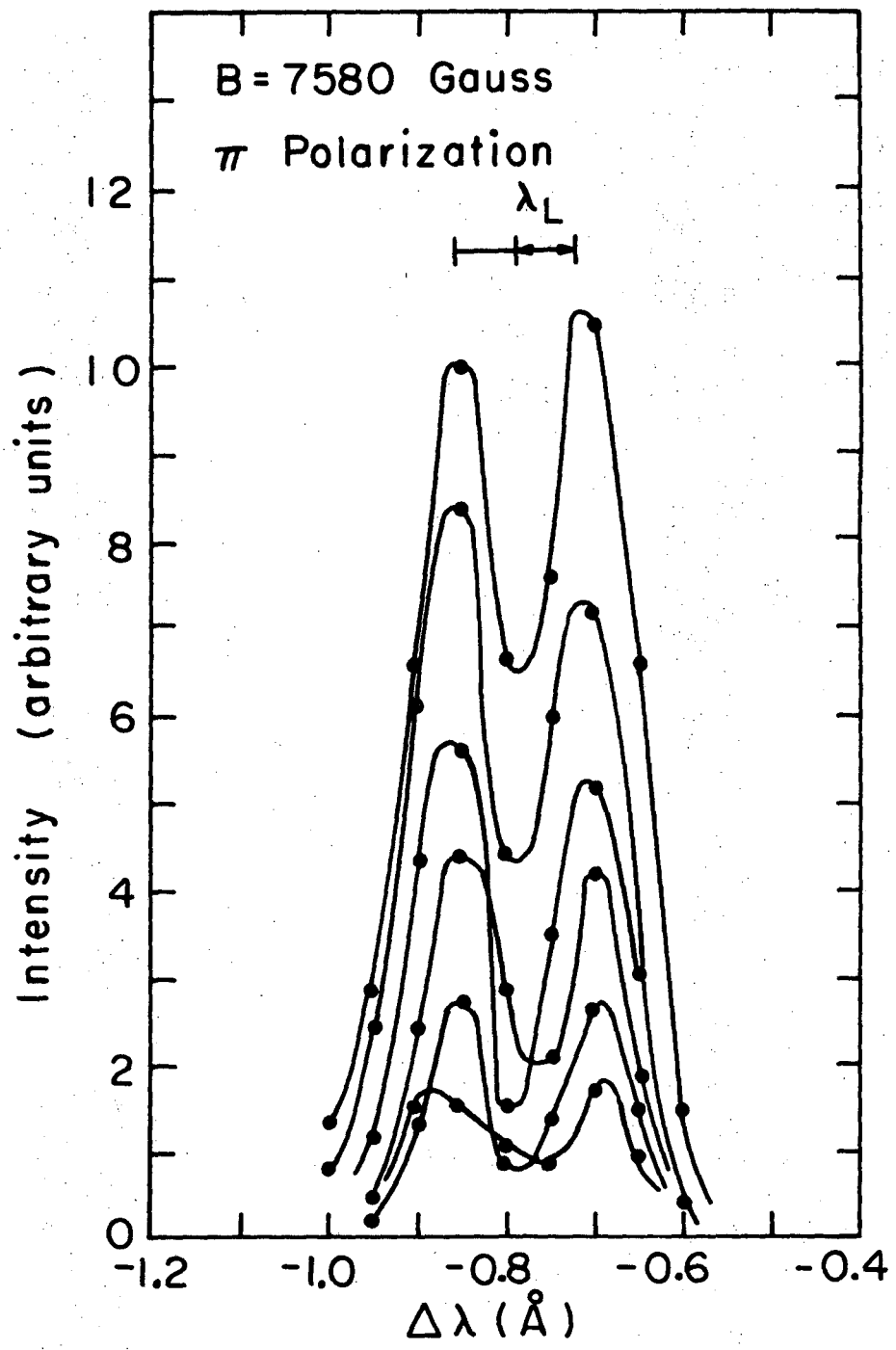

XBL7210-4268

Fig. 19. Data taken at higher magnetic field and slightly different beam parameters than data shown in Figs. 16-18. π polarization of near satellite is shown again at successive 25 nsec intervals.

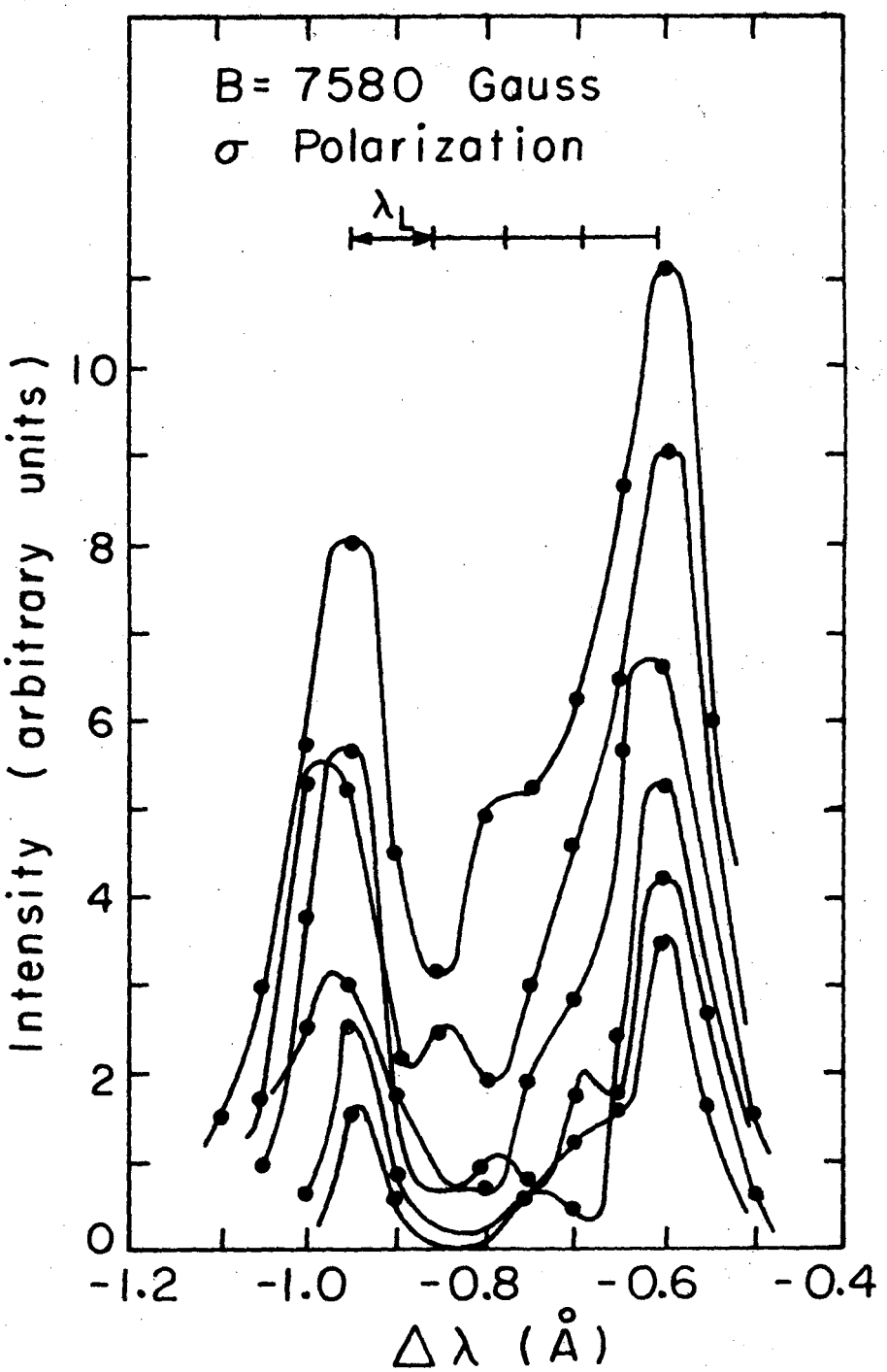

Fig. 20. Same as Fig. 19 except σ polarization is shown.

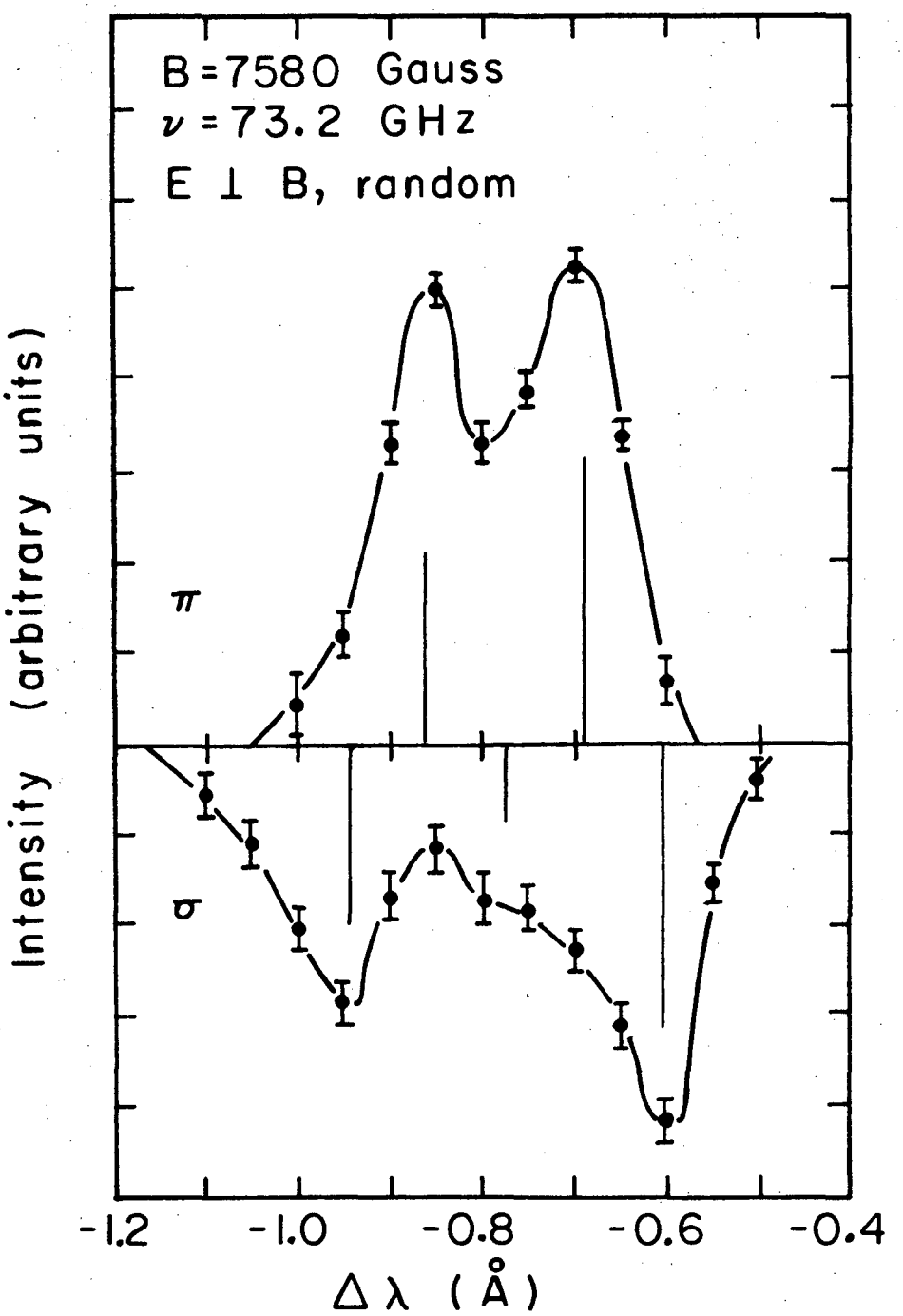

XBL7210-4267

Fig. 21. Same data as Figs. 19 and 20 after electric field had saturated. Dots are experimental points. Vertical bars are theoretical calculations for indicated ν and B, and for an electric field perpendicular to $\vec{B}$ and random in azimuthal angle.

Table II. Plasma parameters.

Peak electron density	5×10^{13} cm^{-3}
Neutral density	1×10^{16} cm^{-3}
Ion temperature	$T_i < 0.15$ eV
Electron temperature	4.4 eV $\lesssim T_e \lesssim$ 22 eV
Electron plasma frequency for peak electron density	6.3×10^{10} Hz
Electron cyclotron frequency	2.0×10^{10} Hz
Upper hybrid frequency	6.7×10^{10} Hz
Ion cyclotron frequency	2.7×10^{6} Hz
Electron-electron collision frequency	1.4×10^{8} sec^{-1}
Ion-ion collision frequency	1.6×10^{9} sec^{-1}
Electron-neutral collision frequency	7.2×10^{8} sec^{-1}
Ion-neutral collision frequency	4.0×10^{6} sec^{-1}
Ion Larmor radius	1.05×10^{-2} cm

T_e = 5 eV, and T_i = 0.05 eV. Spitzer's[55] results for the Coulomb collision time, and the collision cross section on neutral helium given in Brown[56] were used.

The steady state of the beam-plasma system is discussed in Appendix E taking into account ionization due to collisions between neutrals and beam or plasma electrons, and loss of the plasma due to recombination and diffusion; the basic parameters of the plasma are found to be reasonably self-consistent. Ionization in the plasma is produced primarily by collisions between neutral helium atoms and the plasma electrons which are heated by the strong electrick field of the instability; the most significant loss mechanism is diffusion of the charged particles away from the region of the beam.

2. Electric Fields

From the data shown in Fig. 12, it can be seen that there is no time during which the electric field is observed to be growing exponentially. Therefore, the instability that produces the electric field is already in the nonlinear regime within a time of $\lesssim$ 25 nsec after the beam is turned on.

The instability initially grows from noise present in the beam or plasma, and the level of this noise is estimated in Appendix B. The results are that the noise in the beam, which is due to shot noise in the beam current, is about 0.9 V/cm and the noise in the plasma, due to thermal fluctuations in the plasma density, is about 0.12 V/cm. Using the larger of these two values, about 8 e-folds in electric field strength are necessary to reach

the saturation value of 2000 V/cm. The e-folding time can be estimated by assuming the electric field grows exponentially during the entire 25 nsec between beam turn-on and when the electric field is first seen; this yields an e-folding time of 3 nsec.

This result is only a rough upper limit for the e-folding time. It should be remembered that the photons were integrated over time intervals that were 25 nsec long. In Fig. 12 the beam was turned on during Channel 37, but when during that time interval is unknown. Similarly, the electric field grew to an observable level at an unknown time during Channel 38. Thus, the actual time between when the beam is turned on and when the electric fields were first observed could be anywhere from near 0 up to 50 nsec. Also, the 10 nsec that the beam took to turn on must be taken into account. Furthermore, the instability is in the nonlinear regime, where its growth rate is less than exponential, during part of its growth to the level that is measured at Channel 38.

Table III lists the theoretical and experimental values for some of the properties of the electric field. The theoretical value for the temporal growth rate was calculated using Eq. (2), which is correct for the most simple beam-plasma instability--the electrostatic interaction between the beam and the longitudinal plasma oscillations in the case of infinite beam and plasma. Using the results of Seidl,[22] it was found that the beam and plasma temperatures and the collision frequencies were not high enough to effect the temporal growth rate significantly.

Table III. Comparison between theory and experiment for results of the electric field measurements.

	Theory	Experiment
Temporal growth (e-fold time)	0.07 nsec	$\lesssim$ 3 nsec
Spatial growth (e-fold distance)	0.02 cm	1.8 cm
Energy density in the electric field at saturation	1.2 ergs/cm^3	1.8 ergs/cm^3

The spatial growth rate in Table III was calculated using Eq. (7), which is again the growth rate for the electrostatic instability. The electron-neutral collision frequency was used in evaluating Eq. (7). Equation (7), which is valid for an infinite beam and plasma, needs to be modified somewhat due to the finite size of the beam; the results of Self[20] show that for the conditions of the present experiment, the finite size of the beam would decrease the growth rate by a factor of ~ 2. Thus, the e-fold length in Table III would be approximately doubled. Even so, the experimental spatial growth rate, taken from Fig. 14, is must faster than the theoretical growth rate. Actually, since the data in Fig. 14 only cover a factor of 2 in electric field strength, it is probably not valid to assume an exponential growth rate. The spatial growth in the electric field seen in Fig. 14 might be the slow growth after the saturation of the fastest growing mode that was seen by Kainer et al.[28] (Although they were considering the temporal growth, since the instability is convective a similar phenomena will be seen in the spatial growth.)

What may be occurring is that the electrostatic instability grows from the noise level until at some point, perhaps when it begins to saturate, another mode of instability starts to grow until it saturates. This sequence of events could happen several times with only the final mode being observed. However, this behavior is not seen since the Zeeman patterns of the satellites shown in Figs. 16-21 do not change significantly in shape during the 150 nsec that pass from the time the beam is turned on until the

the electric field reaches its final saturated value. Hence, the polarization remains the same during this time, and no change from one interaction mode to another is noticeable.

The presence of the two different polarizations for the electric field in Figs. 16-18 and 19-21 is difficult to explain since they were observed for nearly the same beam parameters. However, many different instabilities are possible since they are caused by coupling between the numerous waves that can exist in the beam and plasma, and the two different polarizations may be due to the instability changing from one type of wave-interaction to another. In order to identify the actual mechanism of the interaction and which wave or waves are present, much more detailed knowledge would be necessary of the properties of the plasma and the electric field.

The fact that the electric field amplitude has its maximum on the edge of the beam rather than at the center can be explained if the beam waves are the surface waves discussed by Self[20] rather than body waves. Self assumes the waves vary as $\exp\left[i(\omega t - m\theta - kz)\right]$ and, depending upon m and k, solutions are found in which either the electric field components parallel or perpendicular to be beam axis predominate, or they may be of approximately equal amplitude; thus these solutions do not conflict with the polarizations that were observed experimentally. In all cases these solutions yield the fact that the electric field is strongest at the edge of the beam; stronger fields would heat the plasma electrons to a higher temperature causing a higher ionization rate

and explaining the higher plasma density at the edge of the beam.

The large uncertainty in the plasma density makes it impossible to decide between several alternatives for the frequency of the interaction. The plasma frequency for a density of 5×10^{13} is 63 GHz, and the error in the density measurement results in an error of ±50% for this frequency. Thus, within errors, the measured frequency of the electric field, 74 GHz, could equal the plasma frequency, the upper hybrid frequency, or some other frequency which might have a more involved dependence upon the plasma and cyclotron frequency and which might also depend upon the spatial size of the system.

The frequency spectrum of the electric field can be determined from the width of the Zeeman components of the spectra seen in Figs. 16-21. The width of these components is due to three effects: the resolution of the optical system; line broadening due to both the Doppler effect and collisions; and the frequency spectrum of the electric field. An estimate of the width due to the first two effects can be gotten from the broadening of the allowed line since it is broadened by the same mechanisms. When the width of the line due to the first two effects was taken into account, the relative bandwidth of the electric field frequency was found to be $\lesssim 14\%$. Thus, the frequency spectrum was quite narrow and remained narrow indefinitely, as the same narrow spectral lines were seen when the electron beam was not modulated. The single-wave model of the linear and initial nonlinear behavior of the beam-plasma instability predicts a narrow spectrum

for the electric field, but the narrow spectrum was still observed at a time beyond which the single-wave model was supposed to be valid. The narrow spectrum of the electric field is also difficult to explain if the frequency of the instability depends strongly on the local value of the plasma frequency since the plasma density changes substantially over the diameter of the beam.

Another comparison that can be made between the nonlinear single-wave theory and experiment is the energy in the electric field. Table III gives the energy in the electric field corresponding to the experimentally measured electric field strength of 2000 V/cm. The theoretical value was calculated using Eq. (16). The relatively good agreement is surprising, again because the instability would be expected to have evolved far beyond the point where the single-wave model was valid.

VI. SUMMARY AND CONCLUSIONS

Spectroscopic measurements have been made on a beam-generated plasma. A strong beam-plasma instability was observed which proved suitable for application of the high-frequency Stark-Zeeman effect to measure the electric fields due to the instability.

The basic plasma parameters of density and electron and ion temperature were measured. The plasma density measured spectroscopically was found to agree within errors with data from Langmuir probes in regions of the plasma outside of the electron beam where both methods could be used.

Taking into account mechanisms for the generation and loss of charged particles from the plasma, the observed density was found to be primarily due to ionization by hot plasma electrons heated by the strong electric fields of the instability; the chief loss mechanism of charged particles was ambipolar diffusion. The electron temperature was calculated several ways and the results were found to be consistent.

The high-frequency Stark-Zeeman effect was used to measure the amplitude, frequency, and polarization of the electric fields due to the beam-plasma interaction. The electric fields were found to have a frequency which could have been the electron plasma frequency or the upper hybrid frequency within errors on the knowledge of the density. The frequency spectrum of the electric fields was estimated from the experimental data and found to be quite narrow. A narrow spectrum is predicted by the single-wave model of the initial nonlinear development of

the beam-plasma instability, but experimentally the narrow spectrum was found to be preserved indefinitely.

The time development of the amplitude of the electric fields was measured. The time resolution of the measurements was insufficient to enable the instability to be observed in the linear regime; when first observed above noise level, the instability was already in the nonlinear regime. The growth rate inferred from this measurement was consistent with the theoretical growth rate for the linear development of the beam-plasma instability. The final saturated amplitude of the electric field agreed quite well with the amplitude predicted by the single-wave model. The electric field was found to have its highest amplitude on the edge of the beam, and the amplitude decreased for both larger and smaller radii. The strong electric fields were also confined to a small region in the axial direction. The radial dependence of the electric field was most likely due to the interaction involving waves on the surface of the beam, rather than body waves.

The polarization of the electric fields was also measured and two distinct cases were observed: in one, the electric field was found to be random in direction, and in the other, the electric field was found to be perpendicular to the magnetic field and random in azimuthal angle. These two polarizations were observed for nearly the same beam and plasma parameters.

In conclusion, the high-frequency Stark-Zeeman effect has proved to be a valuable method for gaining information on the electric fields in a plasma. The data in the present experiment

were not detailed enough to identify the plasma and beam waves that were involved in the beam-plasma interaction, but the polarization of the electric fields ruled out the simple electrostatic instability. The single-wave model, or at least the predictions of it, appear to be valid for times far beyond which it was supposed to apply.

Valuable additional measurements, although probably not feasible with the present apparatus and diagnostic technique, would be measurements on the wavelength of the electric field and information about the instability while it was still in the linear regime.

ACKNOWLEDGMENTS

The author wishes to thank Dr. Wulf B. Kunkel and Dr. William S. Cooper III for their help and guidance throughout the course of this work. The author also wishes to express his thanks to E. B. Hewitt and Barton D. Billard for their assistance in constructing and operating the experimental apparatus, and to Margaret R. Thomas for her help in typing and editing this manuscript.

This work was performed under the auspices of the U. S. Atomic Energy Commission.

APPENDICES

A. Frequently Used Symbols

B	magnetic field strength
E	electric field strength
E_{rms}	root-mean-square electric field strength
k	wave number
k_0	wave number of fastest growing mode
m	azimuthal mode number
n_b	beam electron density
n_p	plasma electron density
S	ratio of intensity of satellite to allowed line
t	time coordinate
T_e	electron temperature
T_i	ion temperature
u	velocity of beam
x	coordinate perpendicular to beam axis
z	coordinate parallel to beam axis
γ	imaginary part of ω = temporal growth rate
γ_0	growth rate of fastest growing mode
η	ratio of beam density to plasma density
θ	azimuthal angle
ν_c	collision frequency
ω	frequency
ω_b	electron plasma frequency of beam

ω_c electron cyclotron frequency

ω_H upper hybrid frequency

ω_p electron plasma frequency of plasma

B. Noise in the Beam and Plasma

The instability due to the beam plasma interaction grows from noise that is present in the beam or plasma. It is necessary to know the frequency dependence of the noise since it is the noise level at the frequency of the most unstable wave which is the initial amplitude of the instability. In the following it is assumed that the simple electrostatic instability grows first and the frequency of the most unstable wave, as given in Eqs. (2), is very close to ω_p. Also, the beam parameters given in Table I, a plasma density of 5×10^{13} cm^{-3}, and a plasma electron temperature of 5 eV will be used in the calculations; the exact values used are not important since only order-of-magnitude results are desired.

1. Noise in the Plasma

The noise in the plasma is primarily due to thermal fluctuations in the charged particle density of the plasma. Bekefi[57] has calculated the energy spectrum of these fluctuations: the result is that the fluctuations are sharply peaked at the electron plasma frequency and the energy per longitudinal wave mode in the electric field in thermal equilibrium is 1/2 T_e (temperature in energy units) for $k\lambda_D \ll 1$, where k is the wavenumber of the mode and λ_D is the Debye length. Using the expression for k_0 given in Eq. (2) and the plasma parameters listed above, $k\lambda_D \cong 2.3 \times 10^{-2}$, so the above condition is well satisfied.

The number of wave modes per unit volume is given simply by

$$dN(k) = \left(\frac{1}{2\pi}\right)^3 d^3k. \tag{B1}$$

Expressing d^3k in spherical coordinates and multiplying by $1/2\ T_e$ we find the energy density to be

$$d\mathcal{E}(k) = \frac{T_e}{2}\left(\frac{1}{2\pi}\right)^3 k^2 dk\ \sin\theta\ d\theta d\phi. \tag{B2}$$

Since we are considering only waves with k parallel to the beam axis, the direction of the fluctuating fields must also considered. If θ is taken to be the angle from an axis parallel to the beam direction, then the component of k along the beam direction will be $k\cos\theta$. Thus, the energy density per wave number in longitudinal waves propagating parallel to the beam axis can be found by multiplying Eq. (B2) by $\cos\theta$ and integrating over θ and ϕ. The result is

$$\frac{1}{8\pi} d\langle \delta E^2 \rangle = \frac{T_e}{2} \frac{1}{(2\pi)^2} k^2 dk, \tag{B3}$$

where δE is the magnitude of the fluctuating electric field.

Again considering the fastest growing mode, the halfwidth of the band of growing wavenumbers, Δk, is given by Eq. (14). Since Δk is small, we let $dk = \Delta k$, and the total energy in the fluctuating fields at the frequency and wavenumber of interest is:

$$\frac{1}{8\pi}\langle \delta E^2 \rangle = \frac{3}{2^{5/6} 8\pi^2} T_e \eta^{1/3} k_0^3. \tag{B4}$$

substituting in numerical values, the result is

$$\delta E = 0.12 \text{ V/cm}. \tag{B5}$$

2. Noise in the Beam

The noise in the beam is due primarily to the shot noise caused by statistical fluctuations in the rate of electron emission from the filament, at least at the frequency of interest. It is not due to thermal fluctuations in the beam since these occur at the beam plasma frequency $\omega_b = \eta^{1/2}\omega_p$. The instability grows at the frequency given in Eq. (2), and when Doppler-shifted to the beam frame gives a frequency of:

$$\omega = \omega_p(1 - 2^{-4/3}\eta^{1/3}) - k_0 u = -2^{-4/3}\eta^{1/3}\omega_p. \tag{B6}$$

Since this is far from the beam plasma frequency, the thermal fluctuations can be neglected, and the shot noise will predominate.

An estimate for the shot noise can be made using the result quoted in Beck[58] for the shot noise in a plane-parallel emission-limited diode:

$$\langle \delta I^2 \rangle = \frac{8eI_0\Delta f}{\omega^2\tau^2}. \tag{B7}$$

Here, δI is the fluctuations in current, I_0 is the total current of the beam, ω is the frequency of the noise, τ is the transit time of an electron between the cathode and anode, Δf is the

bandwidth of the receiver, and it has been assumed that $\omega\tau \gg 1$. The fluctuations in current can be changed to electric field amplitude by using Ohm's law $J = \sigma E$. J is the current density, and σ is the dynamic conductivity for a fully ionized gas:

$$\sigma = \frac{i\omega_b^2}{4\pi\omega} . \tag{B8}$$

Here, $i = \sqrt{-1}$. Using the expression above we find:

$$|\delta E| = \frac{4\pi}{\omega_b^2 A\tau} \sqrt{8eI_0\Delta f} , \tag{B9}$$

where A is the area of the beam.

For the bandwidth, Δf, the half-width of the peak growth rate as given in Eq. (14) is used:

$$\Delta f = \frac{\Delta\omega}{2\pi} = \frac{1}{2\pi} \frac{3}{2^{5/6}} \eta^{1/3}\omega_p . \tag{B10}$$

The transit time which appears in Eq. (B9) was evaluated using the transit time between the cathode and the anode at ground potential. Thus, $\tau \approx 2(12 \text{ cm})/u$, where u is the final beam velocity. The current fluctuations in the beam propagate along the beam in the drift space between the anode and where the beam enters the plasma, but do not change in amplitude.[59] The presence of the grids near the cathode and the space charge in the region between the first grid and cathode also have an effect upon the noise, but the quantitative values of these effects are

difficult to calculate, and the simple theory presented here should be adequate for an order-of-magnitude estimate. Substituting numerical values in Eqs. (B9) and (B10), the magnitude of the electric field is found to be

$$|\delta E| \approx 0.9 \text{ V/cm.} \qquad \text{(B11)}$$

C. Abel Inversion

Abel inversion is a technique to find the local value of the emissivity (watts radiated/steradian/cm^3 of a cylindrically symmetric radiation source from side-on observations. It is assumed that the source is optically thin; that is, there is no reabsorption of the light emitted before it reaches the edge of the plasma. The geometry is shown in Fig. 22. The optical system is assumed to accept photons emitted parallel to the x axis along a thin chord across the plasma cylinder. This is a good assumption for an optical system that has a focal length much larger than the source radius and a small angle of acceptance. The measured light intensity will be:

$$I(y) = 2\int_{y}^{\infty} \frac{\epsilon(r)rdr}{(r^2 - y^2)^{1/2}}, \qquad (C1)$$

where $\epsilon(r)$ is the (desired) local emissivity. This equation can be inverted[60] to obtain:

$$\epsilon(r) = -\frac{1}{\pi}\int_{r}^{\infty} \frac{I'(y)dy}{\sqrt{y^2 - r^2}}, \qquad (C2)$$

where $I'(y)$ is the derivative of I with respect to its argument. For the practical evaluation of Eq. (C2) it is usually important to perform some sort of smoothing operation on the raw data as the presence of the derivative causes error amplification. One technique is to perform a least-square polynomial fit to the data after which the differentiation and integration is done analyti-

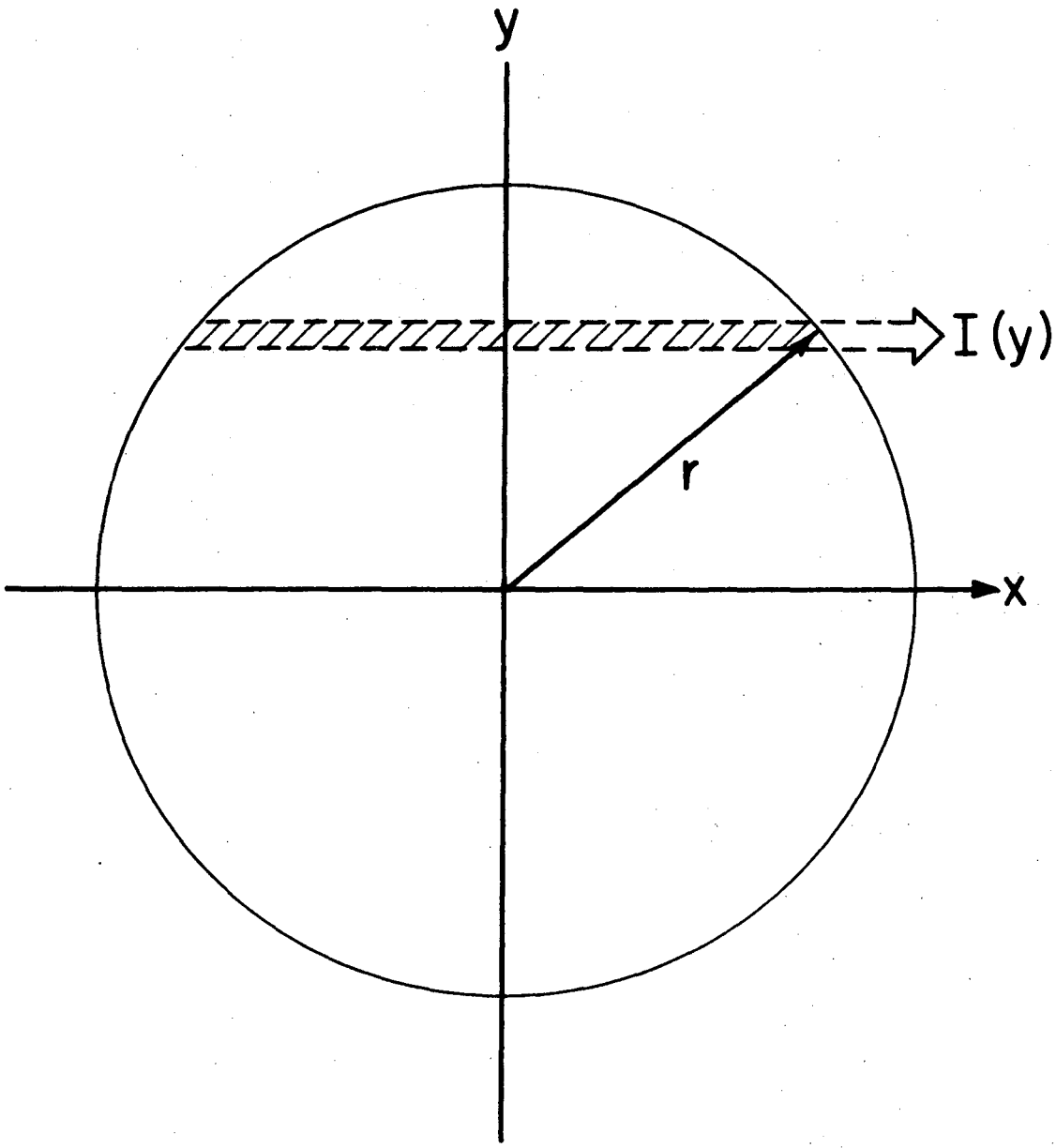

XBL7212-4924

Fig. 22. Schematic view of cylindrical plasma column. I(y) is the light emitted in x direction from the plasma in a narrow chord across the cylinder.

cally. For the present experiment it proved impractical to fit a single polynomial I(y) due to its complex shape, such as is seen in Fig. 11. Consequently, a least-square-fit cubic polynomial was fit between each two data points, using the two data points and the two on either side. Also, as is usually done, data were taken on both sides of the symmetry axis and the results at equal distances from the axis were averaged. This also provides a measure of the validity of the assumption of cylindrical symmetry.

An estimate of the error introduced by the inversion is difficult to make as it depends not only on the method used for inversion but also on the shape of the curve being inverted. What is found empirically is that error in the original data is amplified, with the error being greatest at the center, especially when the intensity at the center is a minimum, as in Fig. 11. For nearly all of the data taken for the present experiment, the two sides of the plasma were symmetric to within ±5%, and an error of this size might result in an error after Abel inversion of 10-20% at the center.

D. Calculation of Plasma Density from Intensity of Forbidden Lines

The intensity of a forbidden line relative to a nearby allowed line can be calculated using Eq. (20) by multiplying the right-hand side by 2 and letting $\omega_0 = 0$. In this case the electric field is due to the quasistatic stochastic fields of the ions and its distribution function is given by the Holtzmark distribution.[61] The most probable field of this distribution is

$$E = 1.6\, E_0, \tag{D1}$$

where E_0 is the "normal" Holtzmark field:

$$E_0 = 2.61\, Zen^{2/3} \approx \left(\frac{4\pi}{3}\, n\right)^{2/3} Ze. \tag{D2}$$

Here, Z is the ionic charge, and n is the ion density. Using Eqs. (D1), (D2), and (20), we can solve for the density:

$$n = 0.267 \left(\frac{m\omega_{ij}}{Z\hbar}\right)^{3/2} R_{ij}^{-3/4} S^{3/4}. \tag{D3}$$

The density as determined by Eq. (D3) is uncertain to within a factor of about 2 due to uncertainty in the choice of the value of the electric field to use in Eq. (D1). Since it is the square of the electric field which appears in Eq. (20), the most obvious choice would to be use the rms electric field rather than the most probable field. Unfortunately, the rms field strength diverges for the Holtzmark distribution since very close encounters between the charged particles are not treated correctly. Some authors[62,63]

use the rms electric field with the integration cut off at the point where perturbation theory breaks down. However, Sadjian et al.[64] used a value for the electric field which was close to the most probable Holtzmark field and in an actual experiment obtained reasonable agreement with other methods for the ion density. Equation (D1) was used since it is probably as valid as the other approach and it simplifies the calculation of the density.

There is further uncertainty in the measurement of the density due to the fact that in the present experiment there are both single and doubly ionized helium atoms present in the plasma. For the results shown in Fig. 9 it was assumed that $Z = 1$, but this would tend to overestimate the density near the center where the doubly ionized He was present. In order to obtain accurate results, the relative densities of He II and He III would have to be known.

E. The Steady-State Beam-Plasma System

The properties of the plasma described in Chapter V are examined below to see if they are reasonable and self-consistent. It is assumed that the plasma is in a steady state, i.e., the parameters of the plasma do not change with time. Only a rough calculation is done since the plasma parameters and their spatial dependence are known only approximately.

In the steady state the equation describing the electron density is:

$$-\nabla\cdot(\vec{\vec{D}}\cdot\nabla n_e) - \alpha n_e^2 + \beta_b + \beta_p = \frac{d}{dt} n_e = 0. \qquad \text{(E1)}$$

Here $\vec{\vec{D}}$ is the ambipolar diffusion tensor, α is the collisional-radiative recombination coefficient, and β_b and β_p are the rate of ionization due to collisions between neutrals and beam and plasma electrons, respectively. All of the above coefficients may depend upon n_e and T_e.

In Eq. (E1) we have ignored the effects of the neutral gas flowing out the hole through which the electron beam enters the plasma chamber. There is a drop in the neutral gas pressure near the hole, but the gradient in the pressure should be significant only for 2 to 3 mm (i.e., 2 to 3 hole diameters) into the chamber and thus would have very little effect on the following calculations.

The first term in (E1) can be approximated by

$$\nabla\cdot(\vec{\vec{D}}\cdot\nabla n_e) \approx \frac{D}{\lambda^2} n_e. \qquad \text{(E2)}$$

λ is a characteristic length of diffusion and $D = \hat{n}\cdot\vec{\vec{D}}\cdot\hat{n}$, where $\hat{n}$ is a unit vector in the direction of diffusion. The transverse diffusion length for a cylinder of radius r is given by McDaniel[65] as $\lambda_\perp = r/2.405$, and using the beam radius yields $\lambda_\perp = 2.1 \times 10^{-2}$ cm. Using the expressions of Golant[66] and the collision frequencies given in Table II, the diffusion constants parallel and perpendicular to the magnetic field are 3.0×10^5 cm^2/sec and 4.5×10^2 cm^2/sec, respectively.

We now consider the plasma produced by the beam alone, i.e., $\beta_p = 0$. Then the plasma will be spatially uniform along the beam, and the longitudinal diffusion length is approximately the length of the chamber: $\lambda_\parallel \approx 30$ cm. For the above values of $\lambda_\parallel$, $\lambda_\perp$, $D_\parallel$, and $D_\perp$, the transverse diffusion predominates and the first term in Eq. (E1) becomes:

$$\frac{D_\perp}{\lambda_\perp^2} n_e = 1 \times 10^6 \, n_e = 5 \times 10^{19} \text{ cm}^{-3} \text{ sec}^{-1}. \qquad \text{(E3)}$$

The value for the collisional-radiative recombination coefficient, α, can be estimated from the results of Refs. 53 and 67. For He at 0.3 Torr, $n_e = 5 \times 10^{13}$ cm^{-3}, $T_e = 5$ eV, α is $\lesssim 10^{-12}$ cm^3/sec. Thus, the recombination term is $\lesssim 2.5 \times 10^{15}$ cm^{-3} sec^{-1} and diffusion will be the dominant loss mechanism in the steady state.

The ionization rate due to beam collisions alone can be calculated from the beam parameters and the mean-free-path for collisional ionization of electrons on He I quoted in Persson;[68] the

result is that $\beta_b = 1.8 \times 10^{18}$ cm^{-3} sec^{-1}. Using this in Eq. (E1) with $\beta_p = 0$ we find

$$n_e = \beta_b \frac{\lambda_\perp^2}{D_\perp} = 1.7 \times 10^{12} \text{ cm}^{-3}. \tag{E4}$$

This is more than an order of magnitude less than the measured density and therefore most of the ionization in the plasma must be due to collisions between neutrals and hot plasma electrons. The ionization rate due to collisions of this type can be calculated using the results of Elwert:[54] for a neutral density of 1×10^{16} cm^{-3},

$$\beta_p = 2 \times 10^8 \, n_e \mu^{-1/2} e^{-\mu} \text{ cm}^{-3} \text{ sec}^{-1}. \tag{E5}$$

Here $\mu = E_I/T_e$, where E_I is the ionization potential of He I.

Since the plasma electrons are heated by the electric fields of the instability, and the electric fields are not uniform along the beam, the ionization rate, and hence the density, will vary along the beam. Thus, the longitudinal diffusion length used above is inappropriate, and if it is assumed that the density approximately follows the strength of the electric field, Fig. 14 yields $\lambda_\parallel \approx 1$ cm. Using this value for $\lambda_\parallel$, the axial diffusion time is

$$\tau_\parallel = \frac{\lambda_\parallel^2}{D_\parallel} \approx 3 \times 10^{-6} \text{ sec}, \tag{E6}$$

while

$$\tau_{\perp} = \frac{\lambda_{\perp}^{2}}{D_{\perp}} \approx 1 \times 10^{-6} \text{ sec.} \qquad \text{(E7)}$$

Thus, these two rates of diffusion are about equal. If the transverse diffusion still predominated, the dip at the center of the density profile in Fig. 9 would be difficult to explain.

Assuming recombination and the ionization due to the beam negligible, Eq. (E1) becomes

$$(-2 \times 10^{8}\ \mu^{-1/2} e^{-\mu} + 1 \times 10^{6}) n_e = 0. \qquad \text{(E8)}$$

Thus, in this case the electron density cannot be determined since both the diffusion and ionization rates are proportional to it. However, the electron temperature can be determined by setting the quantity in the bracket in Eq. (E8) equal to zero and the result is:

$$T_e = 5.4 \text{ eV.} \qquad \text{(E9)}$$

This result is consistent with the estimates for T_e made considering the relative density of He II and He III.

This result for the electron temperature can also be compared with that due to the heating of the electrons by the high frequency electric field. The energy gain per electron in the electric field is:

$$\frac{d}{dt} T_e = \frac{e^2 E_{rms}^2}{m_e} \frac{\nu_c}{\omega^2 + \nu_c^2} . \qquad \text{(E10)}$$

Here ν_c is a damping term due to collisions and ω is the frequency of the field. Since the electrons are only heated until the diffuse out of the region of strong fields, their temperature will be

$$T_e \approx \frac{e^2 E_{rms}^2}{m_e} \frac{\nu_c}{\omega^2} \tau. \tag{E11}$$

Here τ is the diffusion time. Also, we have let $\omega^2 + \nu_c^2 \approx \omega^2$ since the frequency of the electric field is much greater than the electron collision frequencies.

Considering only diffusion perpendicular to the magnetic field, $\tau = \lambda_\perp^2 / D_\perp$. The transverse diffusion coefficient is:[66]

$$D_\perp \simeq \frac{T_e}{m_e} \frac{\nu_c}{\omega_c^2}, \tag{E12}$$

where ω_c is the electron cyclotron frequency. Substituting in (E11) we have

$$T_e = \frac{e^2 E_{rms}^2}{T_e} \lambda_\perp^2 \left(\frac{\omega_c}{\omega}\right)^2, \tag{E13}$$

which yields:

$$T_e = eE_{rms}\lambda_\perp(\omega_c/\omega). \tag{E14}$$

Substituting in the observed frequency and amplitude of 74 GHz and 2000 V/cm, respectively, the electron temperature is found to be

$$T_e \approx 11 \text{ eV}. \qquad \text{(E15)}$$

This is in reasonable agreement with the earlier results considering the approximations that have been made.

REFERENCES

1. Ya. B. Fainberg, The Interaction of Charged Particle Beams with Plasma, Plasma Phys. 4, 203 (1962).

2. Richard J. Briggs, Two-Stream Instabilities, in Advances in Plasma Physics, A. Simon and W. B. Thompson, Eds. (Interscience, New York, 1971), Vol. IV.

3. Richard J. Briggs, Electron-Stream Interaction with Plasmas (MIT Press, Cambridge, Mass., 1964).

4. Irving Langmuir, Scattering of Electrons in Ionized Gases, Phys. Rev. 26, 585 (1925).

5. Lewi Tonks and Irving Langmuir, Oscillations in Ionized Gases, Phys. Rev. 33, 195 (1929).

6. Merrill and Webb, Electron Scattering and Plasma Oscillations, Phys. Rev. 55, 1191 (1939).

7. J. R. Pierce, Possible Fluctuations in Electron Streams Due to Ions, J. Appl. Phys. 19, 231 (1948).

8. J. R. Pierce, Increasing Space Charge Waves, J. Appl. Phys. 20, 1060 (1949).

9. A. V. Haeff, Space Charge Amplification Effects, Phys. Rev. 74, 1532 (1948).

10. A. V. Haeff, The Electron-Wave Tube--A Novel Method of Generation and Amplification of Microwave Energy, Proc. IRE 37, 4 (1949).

11. L. S. Nergaard, Analysis of a Simple Model of a Two-Beam Growing-Wave Tube, RCA Review 9, 585 (1948).

12. D. Bohm and E. P. Gross, Theory of Plasma Oscillations, Phys.

Rev. 75, 1851 (1949).

13. Duncan H. Looney and Sanborn C. Brown, The Excitation of Plasma Oscillations, Phys. Rev. 93, 965 (1954).

14. G. D. Boyd, L. M. Field, and R. W. Gould, Excitation of Plasma Oscillations and Growing Plasma Waves, Phys. Rev. 109, 1393 (1958).

15. I. F. Kharchenko, Ya. B. Fainberg, R. M. Nikolaev, E. A. Kornilov, E. A. Lutsenko, and N. S. Pedenko, Interation of an Electron Beam with a Plasma, Soviet Phys. JETP 11, 493 (1960).

16. James R. Thompson, Nonlinear Evolution of Collisionless Electron Beam-Plasma Systems, Phys. Fluids 14, 1532 (1971).

17. H. Bohmer, J. Chang, and M. Raether, Collision Damping of the High Frequency Instability in a Beam-Plasma System, Plasma Phys. 11, 645 (1969).

18. H. Bohmer, J. Chang, and M. Raether, Influence of Collisions on the Instability of Cold and Warm Electron Beams in a Plasma, Phys. Fluids 14, 150 (1971).

19. C. K. Birdsall, Single-Streaming and Contra-Streaming Instabilities in a Resistive Background, Lawrence Livermore Laboratory Report UCRL-6631, May 1962.

20. S. A. Self, Interaction of a Cylindrical Beam with a Plasma. I. Theory, J. Appl. Phys. 40, 5217 (1969).

21. M. Seidl and P. Sunka, High-Frequence Instabilities in Beam-Generated Plasma, Nucl. Fusion 7, 237 (1967).

22. M. Seidl, Temperature Effects on High-Frequency Beam Plasma

Interaction, Phys. Fluids 13, 966 (1970).

23. W. E. Drummon, J. H. Malmberg, T. M. O'Neil, and J. R. Thompson, Nonlinear Development of the Beam-Plasma Instability, Phys. Fluids 13, 2422 (1970).

24. T. M. O'Neil, J. H. Winfrey, and J. H. Malmberg, Nonlinear Interaction of a Small Cold Beam and a Plasma, Phys. Fluids 14, 1204 (1971).

25. V. D. Shapiro and V. I. Shevchenko, Contribution to the Nonlinear Theory of Relaxation of a Monoenergetic Beam in a Plasma, Soviet Phys. JETP 33, 555 (1971).

26. N. G. Matsiborko, I. N. Onishchenko, V. D. Shapiro, and V. I. Shevchenko, On Non-Linear Theory of Instability of a Mono-Energentic Electron Beam in a Plasma, Plasma Phys. 14, 591 (1972).

27. V. D. Shapiro, Non-Linear Theory of the Interaction of a Mono-Energetic Beam with a Plasma, Soviet Phys. JETP 17, 416 (1963).

28. S. Kainer, J. Dawson, R. Shanny, and T. Coffey, Interaction of a Highly Energetic Electron Beam with a Dense Plasma, Phys. Fluids 15, 493 (1972).

29. I. F. Charchenko, Ya. B. Fainberg, R. M. Nikolaev, E. A. Kornilov, I. I. Lutsenko, and N. S. Pedenko, The Interaction of an Electron Beam with a Plasma in a Magnetic Field, Soviet Phys.-Tech. Phys. 6, 551 (1962).

30. I. F. Kharchenko, Ya. B. Fainberg, R. M. Nikolaev, E. A. Kornilov, E. I. Lutsenko, and N. S. Pedenko, Interaction of

an Electron Beam with a Plasma in a Magnetic Field, in Plasma Physics and Controlled Nuclear Fusion Research, Conference Proceedings, Salzburg 1961, Nucl. Fusion 1962 Suppl., Pt. 3, p. 1101.

31. I. F. Kharchenko, Ya. B. Fainberg, E. A. Kornilov, and N. S. Pedenko, Excitation of Oscillations in Plasma by an Electronic Beam, Soviety Phys.-Tech. Phys. 9, 798 (1964).

32. A. K. Berezin, G. P. Berezina, L. I. Bolotin, and Ya. B. Fainberg, The Interaction of Pulsed High-Current Beams with a Plasma in a Magnetic Field, Plasma Phys. 6, 173 (1964).

33. A. K. Berezin, Ya. B. Fainberg, G. P. Berezina, L. I. Bolotin, and V. G. Stupak, The Interaction of Strong Electron Beams with a Plasma, Plasma Phys. 4, 291 (1962).

34. H. E. Singhaus, Beam-Temperature Effects on the Electrostatic Instability for an Electron Beam Penetrating a Plasma, Phys. Fluids 7, 1534 (1964).

35. S. A. Self, Interaction of Cylindrical Beam with a Plasma II. Experiment and Comparison with Theory, J. Appl. Phys. 40, 5232 (1969).

36. J. R. Apel, Experimental Studies of Linear Beam-Plasma Instabilities in a Magnetic Field, Phys. Fluids 12, 291 (1969).

37. K. W. Gentle and C. W. Roberson, Observation of the Beam-Plasma Instability, Phys. Fluids 14, 2780 (1971).

38. Katsuhiro Mizuno and Shigetoshi Tanaka, Experimental Observation of Nonlinear Wave-Particle Interactions in a Weak Cold Beam-Plasma System, Phys. Rev. Letters 29, 45 (1972).

39. Michel Baranger and Bernard Mozer, Light as a Plasma Probe, Phys. Rev. 123, 25 (1961).

40. Julian Reinheimer, Stark Coupling of Radiation and Plasma Oscillations, J. Quant. Spectrosc. Radiative Transfer 4, 671 (1964).

41. William S. Cooper III and Heinz Ringler, Spectroscopic Measurement of High-Frequency Electric Fields in a Plasma by Observation of Two-Quantum Transitions and Spectral Line Shifts, Phys. Rev. 179, 226 (1969).

42. W. S. Cooper and W. W. Hicks, Use of the High-Frequency Stark Effect in Plasma Diagnostics, Phys. Letters 33A, 188 (1970).

43. William S. Cooper III and Roger A. Hess, Spectroscopic Measurement of the Frequency, Intensity, and Direction of Electric Fields in a Beam-Plasma Interaction by the High-Frequency Stark-Zeeman Effect, Phys. Rev. Letters 25, 433 (1970).

44. William W. Hicks, Roger A. Hess, and William S. Cooper, Combined Zeeman and High-Frequency Stark Effects with Applications to Neutral Helium Lines Useful in Plasma Diagnostics, Phys. Rev. A 5, 490 (1972).

45. J. Brochard and P. Jacquinot, Sur la Nature de Certaines Raies Interdites de l"Helium et l'Interpretations de Leurs Effets Zeeman, Ann. Phys. (Paris) 20, 509 (1945).

46. C. Deutsch, H. W. Drawin, L. Herman, and Nquyen-Hoe, Effets Stark et Zeeman Combines sur les Transitions Hydrogenoides de l'Helium Neutre, J. Quant. Spectrosc. Radiative

Transfer 8, 1027 (1968).

47. H. J. Kunze, H. R. Griem, A. W. DeSilva, G. C. Goldenbaum, and I. J. Spalding, Spectroscopic Investigation of Enhanced Oscillations in a High Voltage Theta Pinch, Phys. Fluids 12, 2669 (1969).

48. F. R. Scott, R. V. Neidigh, J. R. McNally, Jr., and W. S. Cooper III, Use of Optical Spectra to Measure Large Electric Fields in a Hot-Ion Plasma, J. Appl. Phys. 41, 5327 (1970).

49. S. H. Autler and C. H. Townes, Stark Effect in Rapidly Varying Fields, Phys. Rev. 100, 703 (1955).

50. C. F. Burrell and H.-J. Kunze, Two-Photon Absorption and Stimulated Raman Scattering on Excited Helium Atoms in a Plasma, Phys. Rev. Letters 29, 1445 (1972).

51. A. A. Sonin, The Behavior of Free Molecular Cylindrical Langmuir Probes in Supersonic Flows, and Their Application to the Study of the Blunt Body Stagnation Layer, Institute for Aerospace Studies, University of Toronto, UTIAS Report No. 109 (1965).

52. W. S. Cooper III, R. A. Hess, and W. W. Hicks, Spectroscopic Techniques for Measuring High-Frequency Electric Fields in Plasmas, in Controlled Thermonuclear Research Annual Report, July 1969 through June 1970, Lawrence Livermore Laboratory Report UCRL-50002-70, 1970, p. 5-2.

53. E. Hinnov and J. Hirschberg, Electron-Ion Recombination in Dense Plasmas, Phys. Rev. 125, 795 (1962).

54. Elwert, Uber die Ionisations und Rekombinationsprozesse in einem Plasma unde die Ionisationformel der Sonenkorona, Z. Naturforsch. 72, 432 (1952).

55. Lyman Spitzer, Jr., Physics of Fully Ionized Gases (John Wiley and Sons, New York, 1962), p. 133.

56. Sanborn C. Brown, Introduction of Electrical Discharges in Gases (John Wiley and Sons, New York, 1966), p. 10.

57. George Bekefi, Radiation Processes in Plasmas (John Wiley and Sons, New York, 1966), p. 125.

58. A. H. W. Beck, Space Charge Waves (Pergamon Press, New York, 1958), p. 290.

59. L. D. Smullin, Propagation of Distrubances in One-Dimensional Accelerated Structure, J. Appl. Phys. 22, 1496 (1951).

60. Hans Griem, Plasma Spectroscopy (McGraw-Hill Book Company, New York, 1964), p. 176.

61. A. Unsold, Physik der Sternatmosphären, 2nd Ed. (Springer-Verlag, Berlin, 1955), p. 361.

62. Ibid., p. 488

63. Hans Griem, op. cit., p. 556.

64. H. Sadjian, H. K. Wimmel, and H. Margenau, Forbidded Helium Lines in a Plasma Spectrum, J. Quant. Spectrosc. Radiative Transfer 1, 46 (1961).

65. Earl W. McDaniel, Collision Phenomena in Ionized Gases (John Wiley and Sons, New York, 1964).

66. V. E. Golant, Diffusion of Charged Particles in a Plasma in a Magnetic Field, Soviet Phys.-Uspekhi 6, 161 (1963).

67. H. W. Drawin, F. Emard, and H. O. Tittel, Collisional-Radiative Ionization and Recombination Coefficients for Helium Plasmas, in Proceedings of the Ninth International Conference on Phenomena in Ionized Gases, Bucharest, Romania, 1969, p. 2.

68. Karl-Birger Persson, Brush Cathode Plasma--A well-Behaved Plasma, J. Appl. Phys. 36, 3086 (1965).

TECHNICAL INFORMATION DIVISION
LAWRENCE BERKELEY LABORATORY
UNIVERSITY OF CALIFORNIA
BERKELEY, CALIFORNIA 94720